AD-A032 077 GENERAL ELECTRIC CORPORATE RESEARCH AND DEVELOPMENT --ETC F/G 11/9
IMPACT RESPONSE CHARACTERISTICS OF POLYMERIC MATERIALS.(U)
SEP 76 W B HILLIG N00019-75-C-0320
UNCLASSIFIED SRD-76-112 NL

1 OF 1
ADA032077

END

DATE FILMED
1 -77

10

IMPACT RESPONSE CHARACTERISTICS OF POLYMERIC MATERIALS

FINAL REPORT

(1 May 1975 to 30 April 1976)

September 1976

Prepared Under Contract N00019-75-C-0320

For

Naval Air Systems Command
Department of the Navy
Washington, D.C. 20361

By

Corporate Research and Development
General Electric Company
Schenectady, New York

SRD-76-112

Unclassified

SECURITY CLASSIFICATION OF THIS PAGE (When Data Entered)

REPORT DOCUMENTATION PAGE

READ INSTRUCTIONS BEFORE COMPLETING FORM

1. REPORT NUMBER

2. GOVT ACCESSION NO.

3. RECIPIENT'S CATALOG NUMBER

4. TITLE (and Subtitle)
Impact Response Characteristics of Polymeric Materials.

5. TYPE OF REPORT & PERIOD COVERED
Final Report, 1 May 75 to 30 Apr. 76

6. PERFORMING ORG. REPORT NUMBER
SRD-76-112

7. AUTHOR(s)
William B. Hillig

8. CONTRACT OR GRANT NUMBER(s)
N00019-75-C-0320

9. PERFORMING ORGANIZATION NAME AND ADDRESS
General Electric Company
Corporate Research and Development
P.O. Box 8, Schenectady, NY 12301

10. PROGRAM ELEMENT, PROJECT, TASK AREA & WORK UNIT NUMBERS

11. CONTROLLING OFFICE NAME AND ADDRESS
Naval Air Systems Command
Department of the Navy
Washington, DC 20361

12. REPORT DATE
September 1976

13. NUMBER OF PAGES
87 12 88p.

14. MONITORING AGENCY NAME & ADDRESS(if different from Controlling Office)

15. SECURITY CLASS. (of this report)
Unclassified

15a. DECLASSIFICATION/DOWNGRADING SCHEDULE

16. DISTRIBUTION STATEMENT (of this Report)

Approved for public release; distribution unlimited.

17. DISTRIBUTION STATEMENT (of the abstract entered in Block 20, if different from Report)

18. SUPPLEMENTARY NOTES

19. KEY WORDS (Continue on reverse side if necessary and identify by block number)
Ballistic impact
Polymers
Stress relaxation
Indentation

20. ABSTRACT (Continue on reverse side if necessary and identify by block number)
Stress relaxation and creep behavior of PC and PMMA were studied under conditions of constant velocity loading followed by halts. This information was used to deduce relaxation-corrected, force-incursion depth behavior. Measurements of force versus depth were also made on sinusoidally programmed indentation. The evaluation of the "densified" zone forming under the contact area was followed cinematographically. Models were developed including one that leads to the time and velocity dependence of the stress relaxation.

DD FORM 1 JAN 73 1473 EDITION OF 1 NOV 65 IS OBSOLETE

Unclassified

SECURITY CLASSIFICATION OF THIS PAGE (When Data Entered)

406617

TABLE OF CONTENTS

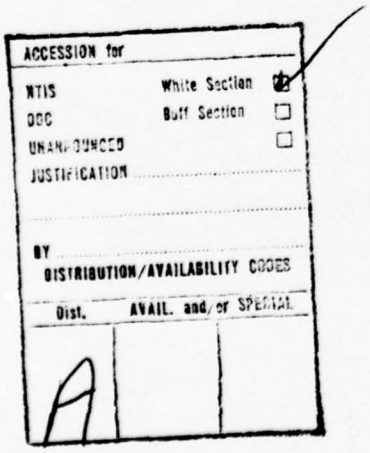

SUMMARY

This report summarizes the work performed in the one-year period beginning May 1, 1975, aimed at developing a basic understanding of the phenomena associated with the impact of small hard objects with polymers such as polycarbonate PC and polymethylmethacrylate PMMA. Whereas previous work was largely aimed at obtaining base data over a wide range of (constant) indentation velocities and penetration depths, the present effort has focused on the exploration of more complex loading conditions in which time effects were explicitly studied. These time dependent effects were deemed more important to impact phenomena than had been suspected, because of the recognition of an unexpected relaxation compensation mechanism that largely masks the time dependent effects under conditions of constant velocity. Hence, changing velocities are required to reveal this basic behavior.

Our objectives for the present work are:

1. Measure the time dependent, stress deformation behavior of PC and PMMA with particular emphasis on systematic measurements down to small indentation depths and on obtaining parametric data for analysis and modeling.
2. Quantify and elucidate the formation of the visibly distinct regions, believed to be compressive yield zones, that form under the indentation/impact area.
3. Develop theoretical and phenomenological models of the impact process that are capable of predicting behavior under complex time-stress-strain conditions and that provide scientific insight.

An additional aim was to extend the impact measurements to greater velocities than are available using electro-hydraulic test machines. The making of a pneumatic impact gun facility was undertaken independently of the contract. However, developing the techniques for the determination of the impact response

by means of an instrumented impact bar was part of the present study.

This report describes the stress relaxation behavior of PC and PMMA following a halt in the incursion process. This was observed over a broad range of conditions. Measurements at very small depths were made to determine how early in the penetration process relaxation effects become significant. The hardening of the material compliance, when the indentation is arrested, was observed on restarting the incursion. These measurements were made as a function of halt duration to determine the effect of history on the material response. Similar measurements were made over a range of depths to define how the relaxation process varies with deformation. Complementary studies were made of the creep recovery of the crater as a function of time under several sets of conditions. Finally, load versus penetration depth was determined for both PC and PMMA under conditions in which the velocity was sinusoidally varied. These combined results provide a relatively complete picture of the relaxation responses over a broad range of conditions. Applying this information to PC and PMMA, it was possible to correct the observed curves of the force versus depth for relaxation effects. This results in the establishment of the instantaneous response curves for these materials.

The growth of the "disturbed" zone under the indentation was followed in PC using a motion picture camera. The zone was found to form virtually from the first moment of contact. The evolution of the geometry of the zone was quantitatively determined from the photographs. The volume of the zone is about 6±1 times the volume displaced by the indenter. Based on this and other information, two qualitatively different estimates were made indicating that the yield stress in PC is between 9 and 29 ksi.

Substantial progress was made obtaining impact pulse data using the instrumented ballistic impact bar apparatus. It was found that a bar made of PMMA gave the best signals because of elimination of the impedance mismatch between the target specimen and the bar material. More work is required to produce an impact pulse of adequate quality to allow computation of force versus penetration depth information.

Finally, a relatively simple molecular model has been formulated which "predicts" the identical stress relaxation law which had been empirically found to provide the best fit of the relaxation data. The model also predicts the experimentally found proportionality between the constant A and the penetration rate (prior to stopping the indenter). However, further work is needed to test the validity of the model under other sets of conditions, such as sinusoidal loading, free impact, etc.

IMPACT RESPONSE CHARACTERISTICS OF POLYMERIC MATERIALS

1. INTRODUCTION

The response of polymers to impact by small hard objects has practical, technological, and scientific interest. There is a need for strong shatterproof windows and impact-resistant polymeric structural members. There is also a need for criteria and characterization parameters for selecting and designing optimal materials and structures. Finally, because the response mechanisms are not well understood in terms of fundamental physical and mechanical material behavior, it is important to develop such understanding. An unraveling of the constituent processes involved in the apparently simple event of a collision could provide a more reliable and interpretable means for characterizing materials and for guiding the synthesis of better impact resistant materials.

This report describes the results achieved during this contract period and builds on the accomplishments[1-3] of the three prior years. Briefly stated, the present work represents a transition between a deliberately simplified set of impact/indentation conditions to a more realistic but complex regime in which the full material-mechanical response is allowed to develop. Throughout the work we have focused on standard, reproducible, commercial polymers of practical interest, viz., polymethylmethacrylate PMMA, polycarbonate PC, and epoxy. The impacting bodies have been spheres or cones. The high symmetry shapes facilitate analysis of the results. The objectives have been to develop a sound reliable set of data covering a wide range of conditions and to develop an understanding of the impact response through analytical models which, in turn, are guided by the experimental results.

1.1 Prior Work

The sustaining focus of the work has been the understanding in depth of the processes that occur at the collision site between the polymer of interest and the colliding object. Because there is a large body of information available on the physico-mechanical behavior of PC and PMMA, the approach was to make as much use of this background as possible. Therefore, measurements were made at low and constant velocities using mechanical test machines. This work showed that the materials did not behave in the expected viscoelastic manner, and some of the analytical work that had been developed did not prove to be as useful as planned. The observed response of the polymers exhibited an unexpected relaxation behavior. Furthermore, the development of a lens-like plastic yield zone of visibly altered material under the site of the impact appears to comprise a major part of the response. These more pioneering aspects of the work are expected to be relevant to other processes, such as the forming of polymer shapes, cold flow processing, and concentrated compressive loading of structural polymers. Because it was necessary to develop a new data base, measurements of force versus penetration depths have been obtained at velocities ranging from 0.0002 to 6000 inches per minute. A 4.5 mm diameter ball bearing (0.177 inches) has been used as the standard reference indenter or projectile. Balls two and four times as large have also been used as well as cones of various apex angles.

Considerable attention has been given to understanding the force penetration behavior. Laws of the form $F = Cx^m R^\alpha$ have been proposed to describe the force F behavior in terms of the diameter of the indenter R and the penetration depth x. The other terms are characteristic constants. When the material is ideally elastic, $C = (4/3)E/(1-\gamma^2)$ where E is the Young's modulus and γ the Poisson ratio of the material; the values of α and m are 1/2 and 3/2 in this case, respectively. This is the behavior we

expected in polymers at large indentation velocities and/or at small indentation depths. The response at high velocities up to or exceeding 300 m per second is an ultimate experimental program goal. The work has focused on getting information in the regimes at which elastic behavior is expected as a reference against which actual behavior can be compared. However, no unambiguously elastic regimes were found. Furthermore, on dimensional grounds ($\alpha + m$) should equal two. However, this value was generally not observed,[3] implying that other unidentified parameters are involved in the impact process.

Among the other major factors being investigated are the time dependence of the response, such as stress relaxation, creep, etc., and the plastic or anelastic yield processes. It has become increasingly evident that the response is strongly history dependent. It was found that the force required to drive an indenter into the polymer is relatively insensitive to the rate of indentation over a span of 7½ decades of the velocity. The reason was not that the apparent elastic modulus was so insensitive to rate but, unexpectedly, was due rather to the dependence of the characteristic stress relaxation time on the prior indentation velocity. At high velocities, the relaxation time was short, whereas at low velocities the relaxation time was long. As a result of these compensating factors for a given penetration depth, the force developed while the indenter is moving is only weakly dependent on velocity.

During a collision between a flying rigid body and the polymer target material (free impact), the projectile velocity constantly decreases because the indentation forces decelerate the projectile. As a result the velocity is an implicitly controlled variable. Thus, studying the force-time penetration under conditions of controlled varying velocity received some preliminary study in the earlier contract efforts. That work indicated that relaxation and history become involved in a somewhat complex way, but that a phenomenological "equation of

state" based on constant velocity data may be useful.[3] The form of this equation for the force F is

$$F = Av^n x^m$$

where v and x are indentation velocity and depth, and A, n, and m are experimentally determined constants.

Finally, the information obtained prior to the present work has been obtained primarily from Instron and MTS mechanical test machines. The former is essentially limited to constant velocity loading at rates up to 20 inches per minute. The latter machine permits loading up to 6000 inches per minute and can be programmed to a wide range of varying velocity-depth-load-time conditions. However, in order to carry the work into the higher velocity regimes requires the use of free impact methods. Some preliminary free impact work using Hopkinson bar techniques has been undertaken to demonstrate feasibility, and some of the procedures outlined for deducing the force penetration response.

With this work as background, the objectives for the present work are as described in the next section.

1.2 Present Objectives

The objectives for the current effort were as follows:

1. Develop the experimental capability for making ballistic impact measurements at velocities up to 300 m per second.
2. Measure the time dependent, stress deformation behavior of PC and PMMA with particular emphasis on systematic measurements down to small indentation depths and on obtaining parametric data for analysis and modeling.
3. Quantify and elucidate the formation of the visually distinct compressive zone to the extent possible.

4. Develop theoretical and phenomenological models of the impact process that are capable of predicting behavior under complex time-stress-strain conditions and that provide scientific insight.

2. MATERIALS AND SPECIMEN PREPARATION

The PC and PMMA materials were unchanged from those used in the previous study. Specimens were used as cut out of sheet stock, making sure that all burrs were removed. The standard specimen size was 1" x 1" x 0.5".

2.1 Polymethylmethacrylate

Specimens were cut from a single sheet of Type G Plexiglas® PMMA (produced by Rohm and Haas). Continuing with our former practice, the sheet was marked off in squares for cutting and a record kept so that the original location of each specimen in the sheet could be identified.

2.2 Polycarbonate

The PC resin was manufactured by the General Electric Company and is designated as Lexan® resin general purpose glazing sheet, Type 9034-112. A single sheet of 0.5" thick material was used, and specimens marked, and records kept as for the case of PMMA.

3. TIME DEPENDENT BEHAVIOR

The interest in behavior such as stress relaxation, creep, and the load deformation behavior under non-constant indentation velocities derives from the requirements for developing a model for free impact. However, more basic questions are involved as well: (1) does the relaxation depend on the amount of deformation; (2) by correcting for the relaxation, is the force versus indentation response unique; (3) are the relaxation and the densification processes related? These questions underlie one of the long-term objectives, viz., the development of a compact, simplified description of the material behavior.

3.1 Relaxation

The present work builds on the information obtained previously and summarized in Tables 3.3.1A-C of the 1975 report in which the load relaxation of PMMA and PC was investigated at 0.002 and 0.2 inches per minute, at two ball sizes, 4.5 and 18 mm diameter, and at depths up to 40 mils at 10 mil increments. The focus of the present work was to investigate the behavior to as small indentation depths as feasible, to investigate the effect of history on the relaxation, and to follow in detail the relaxation behavior in a same specimen over a wide range of indentation depths.

The general procedure has been to force the 4.5 mm ball into the polymer at a fixed rate and to measure the force using a load cell. The output was displayed on a time-base recorder. The depth was determined using the known velocity in combination with the loading time. For some measurements, an extensometer capable of measuring depths to 0.1 mil was used and the output simultaneously recorded. At the desired depths, the screw drive of the test machine was stopped and the decay in force noted. For some experiments the drive was reversed until the load dropped to zero, the purpose being to determine the residual crater depth, as will be described in the next section. After some period of

time at zero load, in these experiments, the drive mechanism was again turned on and the ball driven deeper into the material. In this way various types of information were obtained with a variety of loading histories. The specific variations are discussed below in describing the various experiments.

3.1.1 Small Indentation Depths. Measurements at depths less than 10 mils were undertaken to try to establish the threshold for yield and to see how the character of the relaxation behaves from the point of first contact. For this purpose incremental steps of about 1 mil were made. The fastest loading rate, which still permitted acceptable control of the halt positions, was 0.020 inches per minute. Two series of experiments were performed, in which by turning on the drive mechanisms for 3 seconds the ball advanced about 1 mil. In the one experiment, the drive was stopped for 3 seconds to allow load relaxation, before continuing to advance; and in the second experiment, the pause time was 30 seconds. In this way it is possible to determine the effect of relaxation on the "stiffness" of the polymers, which can be measured from the incremental increase in force with increasing depth when the load is reapplied.

In order to compare, on an equal basis, the increase of load due to increasing penetration depth with the decay of load with time, the data are normalized in terms of the apparent change of force with depth. In other words, regardless of whether the cross-head of the test machine is moving or not, the force is displayed on a strip chart recorder running at constant speed. Hence, when the indentation is halted, the change in force with time can be viewed as if it were a change in force with a change in depth. Thus, column 3 is the observed upward slope of force with actual increase in depth. Column 4 contains the relaxation data, while the indentation is stopped, calculated in terms of the change in force with depth. Column 5 is the time corrected (instantaneous response) slope. This is determined from the

upward slope minus the downward slope, i.e., column 3 plus column 4. Column 6 is the observed upward slope when the indentation is restarted.

The effect of the pause time on the instantaneous response can be seen by reference to Table 3.1.1C which gives the average values for observed startup slope and for the relaxation corrected halt slope. These results show that the startup slope is about 12% greater than the halt slope after 3 seconds of relaxation and about 30% greater after 30 seconds pause duration. This implies a progressive "hardening" of the two polymers as relaxation progresses. However, there is too great a sample-to-sample variation to verify this from the present data. The results for PMMA and PC are given in Tables 3.1.1A and B, respectively.

TABLE 3.1.1 A

Stepwise Indentation of PMMA at 0.020 Inches/Min
with Relaxation Pauses as Indicated

		Halt			Start
1	2	3	4	5	6
x	F	$\frac{dF}{dx}$	$-\frac{1}{u}\frac{\partial F'}{\partial t}$	$\frac{\partial F}{\partial x}$	$\frac{\partial F}{\partial x}$
mils	lbs	lbs/mil	lbs/mil	lbs/mil	lbs/mil
		30 Second Pause Between Steps			
0.7	5.0	7.0	0.2	7.2	11.0
2.1*	15.2	11.8	1.7	13.5	15.0
2.6	28.5	13.0	1.4	14.4	20.0
4.9*	54.0	15.0	5.0	20.0	27.0
6.4	89.5	19.0	8.0	27.0	32.0
9.8*	136.5	19.0	13.0	32.0	37.0
12.3	197.0	19.0	19.0	38.0	39.0
19.2	331.0	17.5	23.0	40.5	--
19.6*	320.0	18.5	27.0	45.5	--
		3 Second Pause Between Steps			
1.3	8.8	9.25	1.60	10.85	11.60
2.5	20.2	10.60	3.65	14.25	15.80
3.7	34.9	12.80	4.95	17.75	19.60
4.8	49.0	14.40	5.10	19.50	23.30
5.7	62.0	16.50	5.20	21.70	23.65
6.9	81.0	18.40	8.85	27.25	28.10
8.0	97.5	20.00	8.70	28.70	--

*Data from one specimen (*) interleaved with data from another (no marking).

TABLE 3.1.1 B

Stepwise Indentation of PC at 0.020 Inches/Min
with Relaxation Pauses as Indicated

		Halt			Start
1	2	3	4	5	6
x	F	$\frac{dF}{dx}$	$-\frac{1}{u}\frac{\partial F'}{\partial t}$	$\frac{\partial F}{\partial x}$	$\frac{\partial F}{\partial x}$
mils	lbs	lbs/mil	lbs/mil	lbs/mil	lbs/mil
		30 Second Pause Between Steps			
0.8	1.0	1.98	0.13	2.11	2.85
2.0	5.1	4.17	0.44	4.61	6.00
3.0	9.8	5.48	0.78	6.26	8.40
4.0	16.2	7.25	1.30	8.55	11.25
5.1	24.5	8.80	1.65	10.45	13.10
6.1	34.1	9.45	2.95	12.40	15.50
7.2	44.6	10.50	3.35	13.85	--
		3 Second Pause Between Steps			
1.0	3.0	3.88	0.30	4.18	4.93
1.9	7.6	5.60	0.60	6.20	7.45
2.9	14.5	7.60	1.20	8.80	7.75
3.8	30.5	8.70	3.00	11.70	14.00
5.0	42.5	9.80	4.05	13.85	--

TABLE 3.1.1 C

Effect of Pause Duration on Averaged Instantaneous Response of PC and PMMA

	Halt	(Ratio)	Start
		PC	
30 Second	5.4	(1.31)	7.1
3 Second	7.7	(1.10)	8.5
		PMMA	
30 Second	13.8	(1.32)	18.3
(Ratio)	(1.13)		(0.96)
3 Second	15.6	(1.14)	17.6

Note: Values are averaged $(\partial F/\partial x)$ using data from Tables A and B for $0<x<5$ mils.

3.1.2 Broad Range of Indentation with Intermediate Pauses. Measurements of the relaxation response were carried out in detail over the range 0 to 50 mils in both PC and PMMA in order to establish the progressive changes that occur in a single specimen. The experiments consisted of indenting the materials at a constant rate, either 0.2 or 0.02 inches per minute, and stopping the process long enough to establish the relaxation constants. The halts were spaced at increasingly larger intervals as the penetration increased. This provides some overlap of information with that in Section 3.1.1 while also extending the data to the practically important large depth regime. The duration of the halts varied, but were typically of the order of the time required to advance the indenter from the previous halt point. The results are given in Tables 3.1.2A and B. Comparison of columns 5 and 6 shows as in 3.1.1 that the instantaneous response slope is substantially greater at startup than at the corresponding halt point. The time decay is best described[3] by the use of the function

$$F(t) = F(o)\ (1 + At)^{-B} \qquad \text{Eq. (a)}$$

where F(t) is the load at a time t since the instant of halt, F(o) is the load when t = 0, and the parameters A and B are experimentally determined constants. Since there are two constants, two conditions are needed to specify their values. One procedure (slope point) is to match the slope at t = 0 with $\partial F'/\partial t$, plus requiring the function to have a given value of F at some particular t. The second procedure (two point) is to require that the function satisfy two values of F for two

particular values of t. The slope-point method would appear to be the more satisfactory. Of course, if the equation truly represents the data and if the data are error free, then the two methods are identical. Practically, it is difficult to measure the slope at t = 0, because the slope of the observed force does not discontinuously change sign when the power to the indenter advance is shut off. This is due to some coasting in the machine, back-lash, time constants in the recording instruments, etc. These points are illustrated in Fig. 3.1.2A, which compares the measured relaxation behavior for a specific example with the results derived by the two methods. As can be seen, the two-point method represents the data better and is the procedure used to produce the values given in Tables 3.1.2C and D. The data are also given in graphical form and are discussed next separately for the two materials.

3.1.2.1 Extended Range Results for PC. The relaxation parameters A and B are plotted as a function of penetration depth x over the range 0-50 mils in Figs. 3.1.2.1A and B, respectively. As can be seen by differentiating Eq. 3.1.2(a), the initial decay slope (column 4 in Tables 3.1.2A and B) is $-F(o)A \cdot B/u$, and the fractional time decay of the force is $-A \cdot B$ (column 5 in Tables 3.1.2C and D). For the case of PC, the tables suggest that the product AB should approach zero as x decreases to zero. Thus, either A or B or both should vanish when x = 0. Fig. 3.1.2.1B indicates that the B parameter is only slightly dependent on x and increases as x decreases. Therefore, A is expected to approach zero, as Fig. 3.1.2.1A shows. As pointed out in the previous report, A is nearly proportional to the indentation velocity u. Although there is considerable scatter in the quantity A/u, a maximum is evident at x = 15±5 mils. The scatter reflects the strong dependence of the computed values of A and B on relatively small

TABLE 3.1.2 A

Values of Time Dependent Force Response Parameters for PC at Incursion Rate of 0.2 and 0.02 Inches/Min

		Halt			Start
1	2	3	4	5	6
x	F	$\frac{dF}{dx}$	$-\frac{1}{u}\frac{\partial F'}{\partial t}$	$\left.\frac{\partial F}{\partial x}\right\|_t$	$\left.\frac{\partial F''}{\partial x}\right\|_t$
mils	lbs	lbs/mil	lbs/mil	lbs/mil	lbs/mil
		0.2 Inches/Min - Specimen 6Q			
4.1	33.0	9.7	0.1	9.8	--
4.6	37.0	4.2	0.0	4.2	15.0
6.0	53.0	13.0	0.4	13.4	13.0
7.2	71.0	14.5	0.8	15.3	14.5
10.3	102.0	11.0	2.0	13.0	16.0
15.1	160.0	12.0	4.3	16.3	20.0
20.1	225.0	10.4	6.0	16.4	35.0
27.5	316.0	11.3	9.4	20.7	35.0
40.4	473.0	10.8	15.0	25.8	45.5
51.8	635.0	9.3	26.3	35.6	--
		0.02 Inches/Min - Specimen 4I			
1.0	6.0	6.5	0.0	6.5	--
2.2	12.7	5.8	0.1	5.9	7.5
3.0	22.0	8.3	0.3	8.6	13.3
4.8	40.0	11.9	1.7	13.6	17.5
7.6	68.5	10.5	3.0	13.5	18.3
9.5	92.0	12.5	6.3	18.8	21.0
13.6	140.0	12.5	10.0	22.5	25.0
20.0	218.0	11.4	12.5	23.9	35.9
28.2	320.0	12.0	19.5	31.5	43.8
41.6	480.0	11.3	27.5	38.5	--

TABLE 3.1.2 B

Values of Time Dependent Force Response Parameters for PMMA at Incursion Rate of 0.2 and 0.02 Inches/Min

		Halt			Start
1	2	3	4	5	6
x	F	$\frac{dF}{dx}$	$-\frac{1}{u}\frac{\partial F'}{\partial t}$	$\frac{\partial F}{\partial x}\Big)_t$	$\frac{\partial F'''}{\partial x}\Big)_t$
mils	lbs	lbs/mil	lbs/mil	lbs/mil	lbs/mil
		0.2 Inches/Min - Specimen 12-O			
0.2	2.0	2.0	0	2.0	5.0
0.6	5.0	4.7	0	4.7	7.0
1.5	9.0	6.9	0.1	7.0	13.0
2.4	26.0	9.7	0.3	10.0	21.0
3.8	46.0	20.0	0.7	20.7	24.0
5.2	68.0	20.0	1.0	21.0	26.0
7.8	118.0	26.0	2.9	28.9	26.0
9.3	136.0	27.0	1.3	28.3	34.0
12.0	195.0	33.0	3.0	33.0	41.0
17.5	330.0	22.5	12.3	34.8	42.5
24.0	477.0	26.3	13.8	42.1	55.0
34.0	710.0	17.9	26.7	44.6	63.0
43.2	900.0	30.0	27.5	57.5	80.0
51.0	1000.0	60.0	18.3	78.3	--
		0.02 Inches/Min - Specimen 10-M			
1.0	10.0	12.5	0.3	12.8	--
2.0	23.6	15.0	0.8	15.8	--
3.4	42.0	18.3	1.7	20.0	22.5
5.6	77.0	18.8	6.3	25.1	31.7
7.6	111.0	23.3	7.5	30.8	35.0
10.0	156.0	25.3	9.4	34.7	41.0
18.2	308.0	18.3	21.3	39.6	50.0
25.0	452.0	20.0	32.5	52.5	62.5
35.0	647.0	15.6	40.5	56.1	65.5
50.0	925.0	14.8	56.3	71.1	--

TABLE 3.1.2 C

Values of Relaxation Constants for PC at Incursion Rate of 0.2 and 0.02 Inches/Min

1 x mils	2 F lbs	3 A	4 B	5 $\frac{1}{F}\frac{\partial F'}{\partial t}\Big)_{calc.}$ min^{-1}	6 $\frac{1}{F}\frac{\partial F'}{\partial t}\Big)_{obs.}$ min^{-1}
	0.2 Inches/Min - Specimen 6Q				
4.1	33.0	68.0	0.025	1.7	0.6
4.6	37.0	--	--	--	0
6.0	53.0	125.0	0.025	3.1	1.5
7.2	71.0	201.0	0.026	5.2	2.3
10.3	102.0	401.0	0.028	11.2	3.9
15.1	160.0	392.0	0.033	12.9	5.4
20.1	225.0	353.0	0.036	11.7	5.3
27.5	316.0	441.0	0.038	16.7	5.9
40.4	473.0	585.0	0.040	23.4	6.3
51.8	635.0	412.0	0.045	18.6	8.3
	0.02 Inches/Min - Specimen 4I				
1.0	6.0	--	--	--	0
2.2	12.7	9.2	0.041	0.4	0.2
3.0	22.0	19.4	0.032	0.6	0.3
4.8	40.0	27.8	0.030	0.8	0.9
7.6	68.5	74.7	0.025	1.9	0.9
9.5	92.0	96.6	0.027	2.6	1.4
13.6	140.0	79.4	0.032	2.5	1.4
20.0	218.0	59.6	0.036	2.1	1.1
28.2	320.0	48.8	0.041	2.0	1.2
41.6	480.0	40.6	0.044	1.8	1.1

TABLE 3.1.2 D

Values of Relaxation Constants for PMMA at Incursion Rate of 0.2 and 0.02 Inches/Min

1 x mils	2 F lbs	3 A	4 B	5 $\frac{1}{F}\frac{\partial F'}{\partial t}\Big)_{calc.}$ min^{-1}	6 $\frac{1}{F}\frac{\partial F'}{\partial t}\Big)_{obs.}$ min^{-1}
	0.2 Inches/Min - Specimen 12-O				
0.2	2.0	--	--		
0.6	5.0	--	--		
1.5	9.0	93.0	0.043	4.0	2.2
2.4	26.0	127.0	0.048	6.1	2.3
3.8	46.0	113.0	0.054	6.1	3.0
5.2	68.0	73.4	0.056	4.1	2.9
7.8	118.0	125.0	0.064	8.0	4.9
9.3	136.0	103.0	0.032	3.3	1.9
12.0	195.0	60.3	0.067	4.0	3.1
17.5	330.0	127.0	0.083	10.5	7.5
24.0	477.0	119.0	0.086	10.2	5.8
34.0	710.0	154.0	0.091	14.0	7.5
43.2	900.0	80.4	0.103	8.3	6.1
51.0	1000.0	44.3	0.098	4.3	3.6
	0.02 Inches/Min - Specimen 10-M				
1.0	10.0	1.45	0.199	0.3	0.6
2.0	23.6	31.2	0.056	1.7	0.7
3.4	42.0	19.9	0.061	1.2	0.8
5.6	77.0	33.1	0.063	2.1	1.6
7.6	111.0	21.5	0.067	1.4	1.4
10.0	156.0	23.1	0.066	1.5	1.2
18.2	308.0	23.7	0.081	1.9	1.4
25.0	452.0	18.7	0.089	1.7	1.4
35.0	647.0	17.2	0.092	1.6	1.3
50.0	925.0	13.5	0.103	1.4	1.2

variations in the input data, as shown in Fig. 3.1.2A, the parameter A being the more sensitive. The variations also reflect the dependence of the relaxation process on deformation history, as well as on the value of deformation at the time of the measurement.

When the calculated decay slope is compared with the value measured directly from the load recorder output, the computed values tend to be substantially larger for both polymers than the measured ones and is seen by comparing columns 5 and 6 in Tables 3.1.2C and D. Using the calculated decay slope in combination with the upward slope at the halt point (column 3 in Table A for the same section) leads to instantaneous response slopes that are in substantial agreement with the corresponding slopes at startup. This is shown in Fig. 3.1.2.1C in which the calculated value for the halt slope $(\partial F/\partial x)_{calc.}$ is compared with the startup slope $\partial F'''/\partial x$. As can be seen, the slope is unity, with modest scatter of the data except for one point. The reason that the curve does not pass through the origin presumably reflects the "hardening" that occurs as the material relaxes as discussed previously in Section 3.1.1.

Finally, in Figs. 3.1.2.1D and E, the dependence of the instantaneous response is given as a function of depth, in terms of Cartesian and log-log plots, respectively. The quantity $\partial F/\partial x$ appears to be a well defined property of the material, at least for the velocity range covered, being relatively insensitive to loading history. This is in contrast to the upward slope, or the relaxation slopes considered separately.

The slope of the log-log plot shows that $\partial F/\partial x$ increases as the square root of the depths up to about 20 mils and then increases linearly with depth. Thus, the behavior is Hertzian initially but shows deviation at higher stress in the direction

of becoming harder. The no-relaxation, force-depth curve can be readily obtained by integrating the plot in Fig. 3.1.2.1D. The Hertz constant derived from this figure is 140,000 corresponding to a modulus value of 315 ksi. These values have been exceeded by our previous measurements at indentation velocities 5 orders of magnitude greater than were used in the present experiments. This implies that the "time independent" behavior shown in Figs. 3.1.2.1D and E is not truly intrinsic, i.e., there must be some residual dependence on velocity.

3.1.2.2 Extended Range Results for PMMA. Although there are some notable distinctions, the behavior of PMMA largely parallels that of PC. Columns 5 and 6 in Table 3.1.2D suggest that although the product AB may be decreasing as x decreases, it may remain finite at the limit, in contrast to the case for PC. Also in contrast are the behaviors of A and B shown in Figs. 3.1.2.2A and B. The quantity A/u behaves more like B in the case of PC, decreasing as x increases from the value at $x = 0$. It also appears to be dependent on indentation velocity. Again, in contrast to PC, it is the B parameter which decreases as x approaches zero. The data are not able to clearly indicate whether or not B vanishes at $x = 0$.

Using the procedure described in the preceding section to determine the relaxation corrected "halt slope," yields values that are in substantial agreement with the startup slope values. This is shown in Fig. 3.1.2.2C. As in the case of PC, the slope is unity and does not pass through the origin, presumably for the same reasons. Figs. 3.1.2.2D and E display the instantaneous response as a function of depth and show that this is a well defined relationship. The log-log curve shows a constant slope of ½ over the entire range, suggesting Hertz-like behavior for this function. The Hertz constant derived from this data is

240,000, from which a modulus of 550 ksi is calculated. To achieve this apparent stiffness in an uninterrupted constant velocity experiment would require a velocity about 10^4 times greater than that used in the present experiment. Since there is a basis for expecting the true time independent modulus to be at least 840 ksi and perhaps as high as 1300 ksi, presumably the present "time corrected" curve must contain hidden time dependent factors. This treatment of the data neglects contributions from plastic deformation processes.

3.1.3 Relaxation Following Uninterrupted Loading. In order to obtain relaxation information on material having simple loading history, measurements, each on a separate specimen, were made in which the ball was driven in at constant velocity with no intermediate pauses until the designated depth was reached. The indenter was then halted and measurements made of the relaxation. Two series of such measurements were made on PC and on PMMA. In the first set of measurements, the ball was always driven into the same depth, nominally 45 mils, but at different velocities (0.002, 0.02, and 0.2 inches per minute), but the depth was varied (nominally 15, 30, and 45 mils). The results are given in Table 3.1.3A. Plots of A/u, B, and $\partial F/\partial x_{calc.}$ are shown in Fig. 3.1.3A as a function of indentation rate for the fixed depth of 45 mils. The figures show that $\partial F/\partial x$ is very nearly independent of rate and give values in good agreement with those presented in Figs. 3.1.2.1D and 3.1.2.1E. However, the behavior of the relaxation constants A and B is somewhat at variance with the results obtained by the progressive interrupted loading of the same specimen as presented in Sections 3.1.2.1 and 3.1.2.2. For example, A/u shows dependence on velocity in the present experiments on PC and little dependence in the case of PMMA, whereas the inverse was observed previously. The values for B lie close to those expected from the previous results.

TABLE 3.1.3 A

Load Relaxation Following Uninterrupted Loading

1	2	3	4	5	6	7	8	9
Sample	u in/min	x mils	F lbs	$\frac{dF}{dx}$ lbs/mil	$-\frac{1}{u}\frac{\partial F}{\partial t}$ lbs/mil	A	B	$\left.\frac{\partial F}{\partial x}\right\|_{calc.}$ lbs/mil
				PC				
4P	0.002	44.7	514	10.0	30.0	1.2	0.084	36.0
8W	0.02	41.9	500	11.2	20.0	34.9	0.049	47.0
10M	0.2	45.0	552	12.5	16.7	260.0	0.045	56.4
				PMMA				
10N	0.002	45.5	755	15.9	44.4	1.06	0.127	66.5
9P	0.02	44.8	792	16.4	40.0	11.1	0.111	64.0
9F	0.2	39.2	780	20.0	30.0	108.0	0.106	64.6
				PC				
8P	0.2	14.6	150	13.3	2.7	281.0	0.021	17.7
8R	0.2	29.3	360	12.7	9.0	473.0	0.038	45.1
8X	0.2	45.0	522	10.8	16.7	330.0	0.043	47.8
				PMMA				
13A	0.2	15.0	290	22.2	10.5	195.7	0.071	42.5
11K	0.2	14.4	285	22.5	6.9	86.5	0.084	32.8
11E	0.2	31.0	600	20.8	20.0	145.7	0.086	58.4
13J	0.2	49.8	970	17.5	34.5	121.6	0.094	72.9

Because there appears to be less scatter in the present data, this suggests that the difference in behavior is real and attributable to differences in loading history. Much more data under carefully controlled conditions would be needed to establish this point.

3.2 Deformation Relaxation

The preceding sections have focused on the load relaxation at an imposed fixed indenter depth. The measurements presented in this section refer to the change in the indentation depth when the load is held constant, or removed altogether. These measurements complement the previous ones in providing a somewhat different mix of the basic molecular relaxation processes and in providing a measure of the non-elastic deformation components. Three series of measurements were made.

In the one series, both PC and PMMA were indented at 0.02 inches per minute to successive depths of 10, 20, 30, 40, and 50 mils. At each of these depths, the indenter was stopped, and load relaxation allowed to proceed for 10 minutes at constant depth. The load was then abruptly reduced to zero, and the residual crater depth measured. This was done by making extensometer measurements simultaneously with the load measurements. The indenter was then advanced at the standard velocity until the next level of indentation depth was attained, and the sequence repeated. Information on the load relaxation can be obtained from this series as well. The data are given in Table 3.2A. The depth of the permanent crater is an increasing fraction of the imposed indentation depth as the latter depth increases. The anelastic strains are comparable in magnitude to the elastic strains. The relaxation parameters are in good agreement with the results obtained in the other series of measurements (see Section 3.1.2).

TABLE 3.2 A

Load Relaxation and Crater Depth Upon Momentary Unload
After 10 Minute Hold at Fixed Depth
Indentation Rate 0.02 Inches/Min

1	2	3	4	5	6	7	8
Applied Depth mils	F lbs	Crater Depth mils	$\frac{dF}{dx}$ lbs/mil	$-\frac{1}{u}\frac{\partial F}{\partial t}$ lbs/mil	A	B	$\left.\frac{\partial F}{\partial x}\right\|_{calc.}$ lbs/mil
			PC - Specimen 7M				
10.0	96.7	2.4	12.0	6.2	88.8	0.029	24.5
20.2	217.0	8.4	13.0	14.0	67.4	0.035	38.5
30.0	335.0	15.5	11.7	20.0	54.9	0.039	47.6
40.2	462.0	23.2	12.5	25.0	49.4	0.041	59.3
50.2	576.0	30.0	12.3	30.0	62.4	0.040	84.2
			PMMA - Specimen 10G				
10.0	108.0	2.1	18.0	8.0	33.2	0.065	29.7
20.2	286.0	7.1	19.2	18.3	22.2	0.079	44.3
30.0	477.0	14.2	20.0	27.5	18.5	0.086	57.9
40.1	680.0	20.0	20.0	36.7	15.7	0.089	67.5
50.0	850.0	27.6	22.5	50.0	14.2	0.091	77.4

It may be possible to use these measurements to arrive finally at an intrinsic description of the material. This might be done by observing the force/depth curves on initial loading, on unloading, and on reloading to the initial depth to determine the magnitude of the various deformation contributions.

The second set of measurements was similar to the preceding set except that the indenter was withdrawn from the specimens by reversing the test machine without pause. The change in the crater depth at zero load was followed for several minutes, whereupon the indenter was advanced to a greater depth and the procedure repeated. The data given in Table 3.2B include the crater depth when the load was first reduced to zero and at the end of the hold time. The short time interval during which the indenter was stationary before reversing the cross-head motion allowed measurement of the initial decay slope, although not of the A and B parameters. The decay slopes are in good agreement with the results previously given in Table 3.1.2A. The curve in Fig. 3.2A shows that the depth recovers very quickly in the early stages of unloading in a manner very similar to the decay of the load when the indenter is abruptly stopped.

The final series of creep recovery experiments consisted of adjusting the penetration depth in order to maintain a fixed load on the indenter. This was done using an Instron mechanical machine equipped to adjust the cross-head position to maintain a load constant to ±10 pounds. The indenter is initially driven in as rapidly as possible using a manual control. The initial incursion rate is estimated to be about 0.2 inches per minute. In the case of PC, the indenter was loaded to fixed values of 153, 353, and 524 pounds, corresponding to initial penetration depths of 14, 30, and 44 mils, respectively. In the case of PMMA, the corresponding load values were 295, 584, and 809 pounds and depths were 16, 28, and 40 mils, respectively. The data for PC and PMMA are shown in Figs. 3.2B and C.

TABLE 3.2 B

Load and Deformation Relaxation Upon Impressing and Immediately Withdrawing the Indenter at 0.020 Inches/Min

1	2	3	4	5	6	7
		Crater Depth				
x	F	Initial	Final	Unload Time	$\frac{dF}{dx}$	$-\frac{1}{u}\frac{\partial F}{\partial t}$
mils	lbs	mils	mils		lbs/mil	lbs/mil
			PC - Specimen 4K			
10.2	98	2.0	0.2	2.75	12.0	5.6
20.2	214	8.8	7.8	2.75	13.0	12.5
30.0	330	15.2	13.7	2.75	12.1	19.5
40.1	455	22.5	20.6	1.35	11.4	26.7
			PMMA - Specimen 12C			
10.1	125	1.9	0.8	1.20	18.7	13.3
20.1	310	5.9	4.0	2.50	20.0	21.3
30.5	505	13.0	9.6	2.50	20.0	30.0
40.5	690	18.1	15.9	2.75	18.6	36.7

After about 1000 seconds, the indenter creep is 10-15% of the initial depth for PC and 25-35% for PMMA. The data for PMMA exhibit superposition, i.e., the creep displacement is proportional to load at any given time. Thus, linear viscoelastic analysis may be applicable and used to develop a Kelvin spring-dashpot model. This is discussed in 6.2. However, in the case of PC, superposition is not obeyed. Hence, such analysis is not valid in this case.

3.3 Sinusoidal Loading

As discussed in the previous report,[3] the use of a time-wise sinusoidal incursion of an indenter into the polymer offers a means of simulating a free ballistic encounter of a projectile with a surface. The objective is to observe the force displacement behavior under these conditions and to try to see how well these can be modeled. For this purpose we made use of an MTS electrohydraulic mechanical test machine which was programmed to give an indentation pulse of the form:

$$x = x_{max} \sin \phi$$

$$= x_{max} \sin \left(\frac{2\pi t}{p}\right) \qquad \text{Eq. (a)}$$

where p is the period and x_{max} the amplitude of the indentation. It is possible to arrange the experiments so that the amount of contact corresponds to $\phi = 0$. Thus, no phase angle correction is needed.

Measurements were made in triplicate on PMMA and PC at periods of 1, 0.1, and 0.02 seconds, the amplitude setting being held fixed at 0.050 inches. The experimental data consist of

simultaneous plots of x and of force versus time. The force as a function of x can be obtained by cross plotting. In order to facilitate this, a computer program was developed. The procedure was as follows:

1. The original curves are digitized by means of an optical-electronic device in which a curve, upon being traced with a stylus, gives rise to an electric output corresponding to the ordinate and abscissa values.

2. These sets of data, one for force the other for displacement, are fed into the computer, which then makes the cross comparisons. The resulting load versus displacement information can be printed or directly plotted.

From the displacement versus time behavior (Eq. b), the instantaneous velocity can be derived by simple differentiation. Thus,

$$v = (2\pi x_{max}/p) \cos (2\pi t/p) \quad . \qquad \text{Eq. (b)}$$

Typical results for PC and PMMA are shown in Figs. 3.3A-D. To a first approximation, the response curve is that corresponding to a constant velocity indentation corresponding to the initial velocity. However, at the maximum incursion depth, significant departures are noted. The calculated curves shown in the figures are derived from a phenomenological model of the force versus depth behavior. This model is discussed in Section 6.3.

4. MATERIAL ALTERATION EFFECTS

The 1975 report noted that a visibly differentiable region develops in the polymer just underneath the indenter contact area. The appearance resembles a transparent bead partially embedded in a transparent matrix. However, the surface is essentially flat as if the exposed part of the bead had been polished away. These zones of "disturbed material" and the associated indentation craters were found to disappear upon annealing. Because the indentation crater that remains is a substantial fraction of the imposed deformation, the creation of this "disturbed" material must represent a major contribution to overall indentation/impact response. The present interest was to determine when and how these regions develop during the incursion process.

4.1 Motion Picture Observations

The most direct way to investigate this was to take motion pictures of the disturbed zone as it developed during the course of an indentation run. For this purpose two side faces of a specimen block of PC were given an optical polish permitting a transverse view of the occurrences within the block.

The test geometry and conditions are as indicated in Fig. 4.1A. The Instron testing machine and the camera were started simultaneously. At the end of the run, the cross head was stopped and about 30 seconds of the relaxation process was photographed. One frame of the motion picture record was printed every 125 frames as an enlargement. A typical photograph is presented in Fig. 4.1B. The contrast marking the boundary of the densified zone is presumably due to the difference in index of refraction between the disturbed and undisturbed material. Measurements of the indenter depth, the depth of the disturbed zone, and the maximum width of

the disturbed zone were made on the photograph. These data are presented in Table 4.1A, and the behavior of the various geometric parameters are plotted in Figs. 4.1C and D.

The viewing conditions made observations very difficult at the earliest stages of the indentation. However, when unambiguous observations did become possible, the behavior was regular so that extrapolation to zero depth appears to be straightforward. The reason for the discontinuity in the depth behavior at 72 second-~60 mil indentation depth is not understood. However, it was very apparent on the picture that at lesser times the growth of the disturbed zone was outracing the advance of the indenter. At greater times, the disturbed zone was just keeping pace with the advance of the indenter. The indenter was halted starting at Photo #26. Interestingly, the disturbed zone shrank during subsequent relaxation.

Fig. 4.1E shows the reconstructed images at 20, 40, and 80 seconds. The semi-major axis a and semi-minor axis b are given in Table 4.1B. Note that the disturbed zone is relatively oblate at small indentation depths and again at very large indentation depths (i.e., a>b), but that it is nearly spherical for intermediate depths. The volume V_c displaced by the indenter and the volume V_z of the disturbed zone were estimated using the standard formula for calculating the volume of a truncated sphere. These values and the ratio of the volumes are given in Table 4.1B. The ratios lie in the range 6±1.

These measurements were difficult and required very careful attention to lighting and geometric arrangement of the camera relative to the specimen; because the geometry was changing during the indentation, the quality of the photographs was not uniform over the entire range of the indentation range. A particular source of difficulty was to determine the position of the indenter itself, because the distortion of the image by the disturbed

TABLE 4.1 A

Geometric Parameters for Indentation Region as Derived from Photographs on Lexan at 0.050 Inches/Min Using 4.5 mm Ball

Photo #	W(max) in	D(zone) in	X(indenter) in	Time(sec)
4	.117	.033	--	20.8
6	.147	.086	.019	31.3
7	.153	.089	--	36.5
8	.163	.107	.026	41.7
9	.177	.115	.028	46.9
10	.186	.130	.031	52.1
11	.198	.142	.033	57.3
12	.211	.153	.036	62.5
13	.224	.159	.042	67.7
14	.236	--	.046	72.9
15	.248	.173	.051	78.1
16	.256	.179	.054	83.3
17	.262	.181	.058	88.5
18	.271	.191	.063	93.8
19	.282	.196	.068	99.0
20	.291	.202	.072	104.2
21	.300	.208	.077	109.4
22	.311	.222	.081	114.6
23	.318	.225	.082	119.8
24	.321	.233	.091	125.0
25	.330	.242	.095	130.2
26	.342	.249	.096	135.4
27	.335	.245	.096	140.6
28	.334	.244	.096	145.8
29	.333	.244	.096	151.0
30	.333	.243	.096	156.3
31	.332	.243	.096	161.5

TABLE 4.1 B

Volumes of Indentation Region

t	x mils	a mils	b mils	V_z $in^3 x10^3$	V_c $in^3 x10^3$	V_z/V_c
20	16.7	57	46	0.38	0.07	5.3
40	33.3	80	80	1.60	0.27	6.0
60	50.0	104	111	4.00	0.56	7.1
80	66.7	125	125	6.60	0.93	7.1
120	100.0	161	143	12.30	1.73	7.1

zone material. Therefore, the indentation depth was calculated from the known time and cross-head speed.

Modeling and further analysis of this data are considered later in Section 6.4. The sharpness of the boundary and its spatial orientation about the indenter suggest association of the interface with an isobar in the sample and in particular, the yield stress.

4.2 Micromechanical Properties of Disturbed Region

Hardness was used as an additional means of characterizing the material in the disturbed zone. Knoop hardness indentation measurements were made on PC and PMMA on the faces of previously indented specimens which were cut and polished on planes which intersected the disturbed zone. The purpose was to see if detectable changes in mechanical properties might result from the structure alteration. In the case of PMMA, there was appreciable random variation in the hardness values. However, there appears to be a trend in the data which indicates a slight hardening at the zone boundary. In the case of the PC, there was a definite hardening of the densified material, again with a suggestion that the effect was greatest at the zone boundary. This is shown in Figs. 4.2A and B. The probable reason the data for PMMA show more scatter relative to that for PC is that cracking occurred in the former material.

Finally, an attempt was made to determine the optical anisotropy and index of refraction in the disturbed region relative to the normal material. However, these measurements were inconclusive using standard refractometric methods. Special apparatus appears to be needed. Hence, this effort was not continued.

5. BALLISTIC IMPACT

A main objective of this continuing study of the impact response of polymers is to measure, analyze, understand, and predict the response of these materials when struck by a projectile. In this situation the velocity, deceleration, reaction forces, penetration depth, etc., are all implicit functions of the projectile shape, mass, velocity, and elastic properties, and of the mechanical response characteristics of the polymer. The 1975 report summarized the results achievable on Instron and MTS mechanical test machines at uniform velocities up to 100 inches per second, the greatest velocity attainable on such apparatus. In the same report and in Section 3.3 of this report are described the intermediate case of a simulated free impact, in which the indenter was programmed to travel at a rate proportional to the cosine of the contact time. In this section we describe the present work on preliminary measurements, observations, and development of the experimental facility for detecting the stress pulse produced by the impact of a freely moving spherical projectile with a polymer specimen mounted on the end of the instrumented impact bar.

The 1972 report[1] discussed the use of such a bar for this purpose. It consists simply of a long bar of uniform circular or square cross section and equipped with some kind of sensor for detecting the impact pulse as it travels down the bar. The bar is free to swing as a pendulum, allowing overall measurements of momentum transfer and providing a potential means for absolute calibration of the stress pulse as detected and recorded. The sensing element is a 1/4-inch long strain gage. Hence, the compliance of the bar must be sufficiently large to produce a readily detectable signal. This suggests a low modulus and small cross section. However, if the strike occurs off center,

then bending vibrational modes will be excited in the bar tending to distort the input signal. This effect can be minimized by use of a stiff bar with a large cross section and by the location of the support points of the bar. Hence, a compromise is required.

The actual new information consists of a voltage versus time signal. The voltage results from the unbalance of the strain gage bridge circuit as the impact pulse travels past the gage. For purposes of analysis, the gage is placed sufficiently far from the struck end to achieve an approximately planar wave strain pulse. Since the impact occurs at a point, the actual pulse is spherical and is further complicated by reflections from the sides of the bar and possible transverse vibrational excitation. Bending can be rendered innocuous by the use of two gages on opposite sides of the bar connected so as to compensate. Other considerations include ensuring that the length of the bar relative to the duration of the impact is adequate to avoid mixing of the reflected pulse from the far end of the bar with the still developing initial pulse. Also, there should be good acoustic matching between the bar and the specimen so that reflections at the bar/specimen interface do not confuse the signal.

Even though the guidelines, as just outlined, are understood there is an unavoidable amount of trial and error effort needed to develop the apparatus to the point where it operates reliably, reproducibly, and gives results that overlap and are in agreement with those previously obtained on the Instron and MTS mechanical test machine. The "diced" steel bar[1] was judged to have too small a cross section (1/4" x 1/4"), and the acoustic impedances of steel and the polymers would be badly matched. Larger bars (1" x 1") of aluminum and PMMA were tried. The metal bar gave too weak a signal to be practical. However, the PMMA bar was

found to give an easily detectable pulse. A 15-inch length bar of the polymer was initially made and was used to establish that attenuation would not be a major problem. The signal strength decayed only about 3% on each traverse. When two such bars were placed end-to-end with a high viscosity acoustic coupling material joining them, an almost clean signal was observed. The bar length must be at least of such a length that the transit time (for the pulse to travel down the rod and return to the site of the strain gage, where it is again detected) is long relative to the duration of the pulse itself. This work shows that a solid PMMA bar of at least 48 inches is required. This will be used in succeeding work.

The impact was produced by striking the impact bar with a 3/4-inch diameter steel ball bearing suspended on the end of a 2 m long filament. The impact velocity was controlled and calculated from the length of the swing, using the well known laws for the motion of a pendulum.

The strain gage was located about 4 inches from the impacted end of the bar, and the signal was recorded in a Nicolet Digital Storage Oscilloscope. This instrument stores the wave shape information in digital form after receiving a pulse that exceeds a selected threshold. By repeated recording, erasing, and re-recording information until such time that a triggering signal is received, the signal shape prior to the trigger point is also preserved. Hence, the important initial stages of the impact pulse can be reliably recorded. This represents a substantial improvement over the instrumentation described in the 1973 report. A typical signal obtained on the longitudinally joined 15-inch bars (equivalent to a 30-inch bar) is shown in Fig. 5A. How this pulse can be analyzed to obtain the inferred force indentation depth behavior is discussed in Section 6.5. It suffices here to point out that this analysis requires various integrations of the pulse shape. Hence, an even more accurate and reliable pulse than obtained to date will be required.

6. MODELING AND ANALYSES

The previous sections presented and treated experimental data from the point of view of describing, quantifying, and comparing the phenomenology. The present section presents analyses and modeling that go beyond the directly observable processes. A model of the relaxation behavior in molecular terms is presented in 6.1. This is obviously speculative in nature. Attempts to relate behavior under various sets of conditions using relatively "simple" phenomenological models are described in 6.2 and 6.3. The following subsection estimates compressive yield stresses from the densification data. Finally, 6.5 discusses how force versus penetration depth information can be determined from impact strain pulse data.

6.1 A Molecular Model of Relaxation

One of the dominant features of the stress relaxation experiments has been the broad range of conditions for PC and PMMA for which the data are fitted well by the empirical law

$$F(t) = F(o)(1 + At)^{-B} \quad .$$

The term F(t) is the force on the indenter at a time t since the penetration was abruptly stopped, F(o) is the force at the instant of stopping, and A and B are experimentally determined constants. The first constant A is found to be proportional, to a very good approximation, to the indentation velocity u prior to stopping, whereas B is essentially independent of u. Both A and B vary somewhat with penetration depth and ball size. Because stress and strain distributions can be expected to vary with penetration depth and ball size, the dependence on geometry is not unexpected. However, the form of the empirical relaxation law and the dependence of A on u does not follow from simple linear viscoelastic theory.

In order to bring more physical meaning to the experimental observations, a theoretical model of the responsible molecular processes has been constructed. The mathematical development is given in the following subsection, and only the qualitative aspects and conclusions are presented here.

The model is guided by the seemingly "thixotropic" behavior of the polymers. That is, once flow commences resistance to flow decreases and upon allowing the system to rest, the resistance to subsequent flow increases with increasing pause time. Therefore, any model must reflect the prior history of the material and must also account for the high rates of flow possible in a glassy polymer at temperatures far below the glass transition. The flow mechanism(s) appears to reflect some kind of cooperative processes. The qualitative concept proposed here is that the glassy polymer consists of coiled intertwined molecular chains, which are effectively prevented from flowing relative to one another, or other segments in the same molecule, because of the high energy barriers and spatial restrictions. However, if a large strain is imposed, then locally some configurational ordering may result allowing relative movement of the segments. This local alignment (or ordering) in turn promotes further ordering. On the other hand, the enhanced mobility also allows the formation of new tangles or "pinned" sites. Thus, the straining leads to "untangling" which increases the ability of the material to flow. That constitutes an increase in the fluidity (reciprocal viscosity) of the system. Hence, it is necessary to focus on the density and on the kinetics of formation or decay of "unpinned" or "ordered" sites relative to the normal immobile "tangled" or "pinned" sites.

The terms "ordered," "pinned," "tangled," and "unpinned" are meant to be broadly descriptive to include geometric hinderances or regions in which secondary chemical binding

locks segments. The details of how this occurs will vary from substance to substance. For the present purpose, it suffices that a density N of "pinnable" sites can be defined and that it is meaningful to consider a site as being in a pinned or unpinned state. Unpinned sites or states will be termed "mobile."

In order to develop a quantitative theory, the following postulates are made:

(1) The fluidity ϕ is determined by two additive terms

$$\phi = \phi_o + Nfa \quad .$$

The term ϕ_o is the classical low strain viscoelastic term. Its absolute magnitude is very small below the glass transition temperature. In the second term, N is the density of pinnable states, f is the fraction unpinned, and a is the fluidity increment per unpinned site per unit volume. That is, the fluidity is assumed to be a linear function of the density of mobile sites.

(2) The time rate of formation of mobile sites is proportional to the strain rate, to the density of mobile sites, and to the density of sites still pinned, i.e.,

$$\frac{df}{dt} = b\dot{\varepsilon}f(1 - f) \quad .$$

The term b is a proportionality constant and can be interpreted as the efficiency factor for unpinning. The linear dependence on f reflects the cooperative assistance to further unpinning due to the presence of nearby ordered (mobile) sites.

(3) The rate of decay (reversion to the pinned state) of mobile sites is proportional to the number of such sites and the fluidity, c being the proportionality constant, i.e.,

$$\frac{df}{dt} = - c\phi f \quad .$$

(4) The net rate of creation (or decay) of mobile sites is given by

$$\frac{df}{dt} = b\dot{\varepsilon}f(1 - f) - c\phi f \quad .$$

(5) When an imposed strain rate initially held constant for an extended time is suddenly reduced to zero, the stored elastic strain energy continues to produce plastic strain. This causes the elastic strain to decrease and decreases the force necessary to maintain the total strain constant. The plastic and elastic responses can be considered to be mechanically coupled in series. Hence, the force F is

$$F = K\varepsilon_{el}$$
$$= J\dot{\varepsilon}_p/\phi$$

where K is a constant which reflects the elastic modulus of the polymer and the geometry of the loading system, J is a constant which reflects the geometry of plastic region, ε_{el} is the elastic strain, and $\dot{\varepsilon}_p$ is the plastic strain rate.

Mathematical connection between these postulates leads to the following result:

$$F(t) = F(o)(1 + At)^{-B}$$

in which $A = Nabc\dot{\varepsilon}/(b\dot{\varepsilon} + Nac)$

and $B = K/Jc$.

Finally, for the ball indentation situation, the strain rate can be assumed to be proportional to the indentation velocity u. The agreement of the form of this equation with the experimentally observed laws is apparent. If $Nac >> b\dot{\varepsilon}$, then the observed proportionality of A on u, i.e., on $\dot{\varepsilon}$, is "explained." The constants A

and B are expected on the basis of this model to be weakly dependent on geometry. The model predicts that for a sufficiently high indentation velocity $b\dot{\varepsilon}$ will exceed Nac, in which case the relaxation parameter A will become independent of velocity. Thus, a new kind of indentation/impact behavior would be expected.

This model is in the early stages of development. Testing is needed to see whether:

(1) Its various predictions correspond to known fact;

(2) The values of the various constants are reasonable;

(3) A simple concept of this kind, which is based on only one state variable f can account for the various kinds of complex deformation responses;

(4) A more detailed consideration of the complex stress-strain contours around a spherical indenter will modify the conclusions.

6.1.1 Mathematical Development of the Molecular Model of Stress Relaxation. The postulates and definitions of the terms have been given in the above Section 6.1.

The fluidity ϕ is assumed to be representable by:

$$\phi = \phi_o + Nfa \quad . \qquad \text{Eq. (a)}$$

The net rate df/dt of formation of mobile sites is given by:

$$\frac{df}{dt} = b\dot{\varepsilon}f(1 - f) - c\phi f \quad . \qquad \text{Eq. (b)}$$

When the strain rate $\dot{\varepsilon}$ has been held constant for a long time, or is only varying slowly, then

$$\frac{df}{dt} = 0$$

or

$$b\dot{\varepsilon}(1 - f) = c\phi \quad . \qquad \text{Eq. (c)}$$

This can be used to define f_{ss} the steady state fraction of mobile states.

Now let $\dot{\varepsilon}$ be abruptly reduced to zero from its previous steady state level. In order to consider how the applied load relaxes, the elastic and visco-plastic components of the stress supporting that load can be considered to be in series. The plastic flow due to the applied forces creates a balancing "viscous drag" force. This, in turn, is supported elastically by the non-flowing material. Hence,

$$\varepsilon = \varepsilon_{el} + \varepsilon_{p} \qquad \text{Eq. (d)}$$

$$\dot{\varepsilon} = \dot{\varepsilon}_{el} + \dot{\varepsilon}_{pl} \qquad \text{Eq. (e)}$$

where ε is strain, the subscripts identify elastic or plastic components, and $\dot{\varepsilon}$ is strain rate. The resisting force F is given by

$$F = K\varepsilon_{el} \qquad \text{Eq. (f)}$$

$$= J\dot{\varepsilon}_{p}/\phi \qquad \text{Eq. (g)}$$

When the indenter is stopped $\dot{\varepsilon} = 0$, or

$$\dot{\varepsilon}_{el} = - \dot{\varepsilon}_{p}$$

Therefore,

$$K\varepsilon_{el} = - J\dot{\varepsilon}_{el}/\phi \quad , \qquad \text{Eq. (h)}$$

the solution of which is

$$\ln \frac{\varepsilon}{\varepsilon_{o}} = - (K/J) \int_{o}^{t} \phi dt \quad . \qquad \text{Eq. (i)}$$

An expression for the time dependence of ϕ is now required. This can be done by substituting Eq. (a) into Eq. (b) and setting $\dot{\varepsilon} = 0$. Because ϕ_o is expected to be very small, it is neglected here. This results in a considerable mathematical simplification. The modified Eq. (b) is thus

$$\frac{df}{dt} = - Nacf^2 \quad , \qquad \text{Eq. (j)}$$

the solution of which is

$$f = \frac{f_{ss}}{1 + Nacf_{ss}t} \qquad \text{Eq. (k)}$$

Introducing this into Eq. (a) yields:

$$\phi = \frac{Naf_{ss}}{1 + Nacf_{ss}t} \qquad \text{Eq. (l)}$$

This is the expression required to carry out the integration in Eq. (i) to give:

$$\ln \frac{\varepsilon}{\varepsilon_o} = - (K/Jc)\ln(1 + Nacf_{ss}t) \quad .$$

Note that

$$\frac{\varepsilon}{\varepsilon_o} = \frac{K\varepsilon}{K\varepsilon_o} = \frac{F}{F(o)} \qquad \text{Eq. (m)}$$

or $$F = F(o)(1 + At)^{-B} \qquad \text{Eq. (n)}$$

where $$A = Nacf_{ss} \qquad \text{Eq. (o)}$$

and $$B = (K/Jc) \quad . \qquad \text{Eq. (p)}$$

Now f_{ss} can be given in terms of $\dot{\varepsilon}$ by combining Eq. (a) and Eq. (c). Nevertheless ϕ_o as before finally gives:

$$f_{ss} = b\dot{\varepsilon}/(Nac + b\dot{\varepsilon}) \quad . \qquad \text{Eq. (q)}$$

Therefore, A can be expressed in terms of $\dot{\varepsilon}$ as

$$A = Nabc\dot{\varepsilon}/(Nac + b\dot{\varepsilon}) \quad . \qquad \text{Eq. (r)}$$

Now for the case of a ball being impressed into a planar target, it is reasonable to relate $\dot{\varepsilon}$ to the indentation velocity u through

$$\dot{\varepsilon} = gu \quad , \qquad \text{Eq. (s)}$$

where g is a proportionality constant that depends on the ball size, the penetration depth, and probably the material. Therefore A can also be expressed in terms of u by a simple substitution, and for

$$Nac >> bgu$$

gives

$$A \simeq bgu \quad . \qquad \text{Eq. (t)}$$

This completes the derivation.

6.2 Spring-Dashpot Model of PMMA Response

The compressive creep behavior of PMMA when subjected to a constant load of 295, 584, and 809 pounds was presented in Section 3.2.

The focus of this section is to examine to what extent this kind of data can be used to predict the response when the loading or deformation conditions are quite different. Spring-dashpot

models are very useful[4] for such purposes in the case of linear viscoelastic materials. Even though we have found significant departures from viscoelastic response in the indentation/impact measurements, nevertheless in many qualitative respects the response is as classically expected. Therefore, we have analyzed the creep response in terms of a fairly sophisticated 7 element spring-dashpot model, and then used this to compute the expected response under conditions of constant indentation velocity. The model is shown in Fig. 6.2A. Its response in terms of deformation at constant load (i.e., creep) is given by

$$\frac{\Delta x}{F} = D(t) = \frac{1}{M_e} + \sum_{i=1}^{3} \frac{1}{M_i} \left(1 - e^{-t/\tau_i}\right) \quad .$$

Thus, seven independent constants are used to describe the data. These are determined by analyzing the creep response as a function of time and load. The best fit is given by the following values:

$M_e = 1.98 \times 10^4$ $\qquad$ $\tau_1 = 10$

$M_1 = 5.56 \times 10^6$ $\qquad$ $\tau_2 = 31.6$

$M_2 = 1.76 \times 10^7$ $\qquad$ $\tau_3 = 316.2$

$M_3 = 2.49 \times 10^7$

The procedure[4] for solving for these values is somewhat involved and will not be discussed here. These constants can now be used, assuming linear viscoelastic response to predict behavior under conditions of stress relaxation or

constant indentation velocity, etc. New expressions often quite complicated must be developed for these other conditions. This can be done using the method of Laplace transforms. Applying the present results to the case of constant indentation velocity gives:

$$F(t) = R \cdot 1.983 \times 10^{4} \left[46.4 + .76t + .155e^{-\alpha t} - 43.8e^{-\beta t} - 2.8e^{-\gamma t}\right]$$

where R is the indentation rate in inches per second, and

$$\alpha = 1.04 \times 10^{-1}$$
$$\beta = 3.9 \times 10^{-3}$$
$$\gamma = 3.27 \times 10^{-2} \quad .$$

The results of this model are compared with the experimental data shown in Fig. 6.2B for an indentation rate of 0.002 inches per minute. At least under these conditions, the results are in good agreement. At short times this expression can be approximated by $F(t) = R \cdot 1.983 \times 10^{4} \cdot 1.006t$. Since $x = Rt$, it follows that this model predicts the force to be independent of velocity at small indentation depths. This model cannot be expected to be valid at velocities greater than that used to initially load the creep specimens. While the results are encouraging, further work would be needed to establish the validity of this approach under a wide range of conditions.

6.3 Application of Equation of State to Sinusoidal Indentations

The ability to program the indentation so that the penetration is proportional to $\sin 2\pi t/p$, where t is time and p is the period, can be used to approximate a free ballistic impact between a ball projectile and the target. In the case of a free ballistic impact, the force-time-depth relationships are

determined by the implicit balance between the inertial force and the reaction forces in the material. In the sinusoidal impact, the incursion is explicitly controlled. Hence, it is of considerable importance to be able to predict the reaction force as a function of time and depth under conditions in which velocity is continuously changing.

From the measurements at constant velocity, it has been possible to describe the results by the empirical laws:

$$F = 23380\ u^{.0290}\ x^{1.187} \quad \text{(PC)}$$

$$= 34670\ u^{.0596}\ x^{1.143} \quad \text{(PMMA)}$$

in which u is velocity in inches per minute and x penetration depth in inches. Therefore, it was of interest to determine how well these relationships predicted the response under sinusoidal deformation conditions. The experimental results for PC are compared with the calculated vales in Figs. 3.3A and B for the case of imposed periods of 0.02 and 0.1 seconds, respectively. The corresponding results for PMMA are given in Figs. 3.3C and D. Part of the discrepancy is due to the uncertainty of the position in the sinusoidal cycle at which the indenter first contacts the target material. The main effect of this uncertainty is to shift the response curve along the abscissa relative to the ideal calculated curve. Except for such translational effects, the agreement between the computed and the measured values is within experimental error for depths as great as about 70% of the full amplitude. At greater depths the experimental values of the force show a gradual drop off away from a linear force versus depth response. In contrast, the computed curve remains linear to greater depths but then shows a very steep drop as u approaches zero. The agreement

at the initial stages of contact suggests that this approach can be useful to model this regime.

6.4 Yield Stress Estimation for PC

In Section 4.3 of the previous report, the disturbed zone that was noted to form under the indentation site (see Section 4.1 of present report) was interpreted as being a yielded region. The yield stress can be estimated by two independent methods. The one considers the region under the indenter to be hydrostatically compressed at a pressure p. Thus, the force exerted by the compressed region on an indenter of radius R at an indentation depth x is given by

$$F = 2\pi Rxp \qquad \text{Eq. (a)}$$

From the known slope of the indentation force with penetration depth dF/dx, the pressure p can be computed. The yield stress Y following Hill[5] is related to p by

$$p = \frac{2Y}{3}\left(1 + \ln \frac{E}{3(1-\gamma)Y}\right) \qquad \text{Eq. (b)}$$

In the earlier report, the yield stress was inadvertently omitted from the denominator in the ln term, leading to an incorrect computation for Y in the previous report. Making use of the experimental slopes dF/dx, taking the Poisson ratio for both PC and PMMA to be 0.35, and the Young's moduli to be 350,000 and 420,000 psi for PC and PMMA respectively, leads to the following corrected values for the yield stress.

	Velocity inches/min	dF/dx ksi/in	Y ksi	Y/E
PC	0.002	13	8.7	0.025
	0.2	13	8.7	0.025
PMMA	0.002	18.3	12.9	0.031
	0.2	22.3	17.0	0.040

The second method also based on the results of Hill[5] makes use of the size of the yield zone relative to the size of the cavity (crater) produced by the indenter. This is discussed in the previous report. The required expression is

$$V_c = 3(1 - \gamma)\, V_z\, (Y/E) \qquad \text{Eq. (c)}$$

where V_c is the volume of the cavity, and V_z is the volume of the yielded zone. As was discussed in Section 4.1, the size of the cavity decreases markedly when the indenter is removed. The values of V_c and V_z of concern are those when the compressive load is applied. Hence, when the values observed in the unloaded condition are used to compute (Y/E) as described in the previous report, the computed value must be considered to represent a lower bound estimate. The value of V_z/V_e under load is given in Table 4.1B and is equal to 6.2±0.9 for PC at 0.050 inches per minute indentation velocity. This leads to a value of Y/E of 0.083 corresponding to a yield stress of 29 ksi for PC.

Both of these methods of estimation are based on calculations for situations that do not actually correspond to the case of the indentation. The pressure model in effect requires that there be no friction between the indenter and the polymer. The displaced volume method assumes spherical symmetry, again

with no friction at the interface. Therefore, both methods have weaknesses. However, the fact that the force is observed to be proportional to $R^{0.45\pm0.15}$ instead of R, as predicted by Eq. (a), suggests that the estimate based on the pressure concept is the less reliable.

6.5 Determination of Force Versus Indentation Depth From Impact Pulse Measurements

This section outlines the treatment of data required to interpret the impact pulse, observed when a projectile strikes the polymer target mounted on an instrumented impact bar. The information desired is the material's response, i.e., the force versus penetration depth.

Because the impact occurs over a concentrated area, the compressive acoustic pulse radiates initially as a spherical wave pocket. As the compressive wave travels down the bar, it becomes increasingly planar. However, if the initial impact did not occur on the axis of symmetry of the bar, then flexural modes can be excited in the bar. Furthermore, surface waves can be expected as well as transverse waves, generated due to Poisson effects and reflections. Thus, the signal detected by the strain sensor reflects a complex super position of wave components. In spite of this, the treatment of the data will be made as if the strain pulse consisted only of planar wave components. This means the analysis will be somewhat in error and that some means of independent calibration to provide the necessary corrections would be desirable.

To carry out the analysis, it is convenient to refer to the position of the struck end of the bar as the origin of the z axis and the time $t = 0$ at the instant of first contact between the ball and the bar. The ball is assumed to be incompressible and to have a mass m.

Deceleration of the spherical projectile results from the local opposing material reaction force which in turn is supported elastically in the impact bar. Hence, the instantaneous deceleration force is $A\sigma(t)$ where A is the cross section of the bar, and σ the longitudinal stress (assumed uniform over the cross section). Therefore,

$$m\ddot{z} = - A\sigma(t) \qquad \text{Eq. (a)}$$

$$= - AE\varepsilon(t) \quad . \qquad \text{Eq. (b)}$$

This can be integrated immediately to give

$$\dot{z} = - (AE/m) \int_o^t \varepsilon dt + v_o \quad , \qquad \text{Eq. (c)}$$

and

$$z = v_o t - \frac{AE}{m} \int_o^t \int_o^{t'} \varepsilon dt' dt \qquad \text{Eq. (d)}$$

where E is the Young's modulus of the bar, ε is strain, and v_o is the initial velocity of the projectile. However, the collision causes the impact bar to be elastically compressed. Therefore, the end of the bar is displaced in the direction of the impacting projectile a distance w

$$w = \int_o^z \varepsilon dz \qquad \text{Eq. (e)}$$

$$= c \int_o^t \varepsilon dt \qquad \text{Eq. } (e^1)$$

where c is the velocity of sound. Thus, the penetration is given by

$$x = z - w \qquad \text{Eq. (f)}$$

and the velocity of the projectile relative to the end of the bar is given by

$$\dot{x} = \dot{z} - c\varepsilon \qquad \text{Eq. (g)}$$

Assuming the projectile to rebound with a velocity v_f, its change in momentum must equal the momentum impacted to the bar. This is the total time integral of the force (neglecting reflections), or

$$m(v_o + v_f) = AE \int_o^\infty \varepsilon dt \quad . \qquad \text{Eq. (h)}$$

Thus, (c) becomes

$$\dot{z} = (AE/m)\left[\frac{v_o}{v_o + v_f} \int_o^\infty \varepsilon dt - \int_o^t \varepsilon dt\right] \quad . \quad \text{Eq. (i)}$$

Thus, in principle the velocity of the impact x (u using previous notation), the depth of the penetration x, and the resisting force $F = AE\varepsilon$, can all be computed from the impact pulse.

In general the actual measurement of the pulse consists of a strain gage voltage reading as a function of time. This strain is presumably proportional to the strain averaged over the cross section. However, for reasons already discussed, strain at the gage itself can be expected to depart from the average strain.

If $\varepsilon_{gage} = \beta\varepsilon_{ave.}$, then the value of β can be determined using Eq. (h) using independently measured values of m, v_o, A_1 and E in conjunction with the total pulse area in the strain-time curve.

Preliminary attempts to apply these equations to the observed pulses indicate that further refinement of the pulse to eliminate artifacts and contributions from non-planar modes is required.

7. ACKNOWLEDGMENT

The principal investigator appreciates and acknowledges the combined experimental contributions of R. L. Mehan, W. P. Minnear and very extensively of G. F. Selden. In addition the analyses of the Kelvin model and the application of the equation of state to the sinusoidal model were performed by Mr. Mehan. This work has also benefited from discussions with R. P. Kambour, D. G. LeGrand and A. F. Yee.

8. REFERENCES

1. W.B. Hillig, "Impact Studies of Polymeric Matrices," General Electric CRD Report SRD-73-091, prepared under Contract N00019-72-C-0218 for Naval Air Systems Command, Dept. of the Navy, March 1973.

2. W.B. Hillig, "Impact Response Characteristics of Polymeric Matrices," General Electric CRD Report SRD-74-087, prepared under Contract N00019-73-C-0282 for Naval Air Systems Command, Dept. of the Navy, September 1974.

3. W.B. Hillig, "Impact Response Characteristics of Polymeric Matrices," General Electric CRD Report SRD-75-083, prepared under Contract N00019-74-C-0147 for Naval Air Systems Command, Dept. of the Navy, August 1975.

4. R.L. Mehan, "Viscoelastic Characterization of Phenolic Nylon by Means of a Five-Element Kelvin Model," Am. Soc. of Mech. Engrs., Paper #64-WA/RP-6, 1964.

5. R. Hill, The Mathematical Theory of Plasticity, Oxford Univ. Press, London, 1950, p. 97 ff.

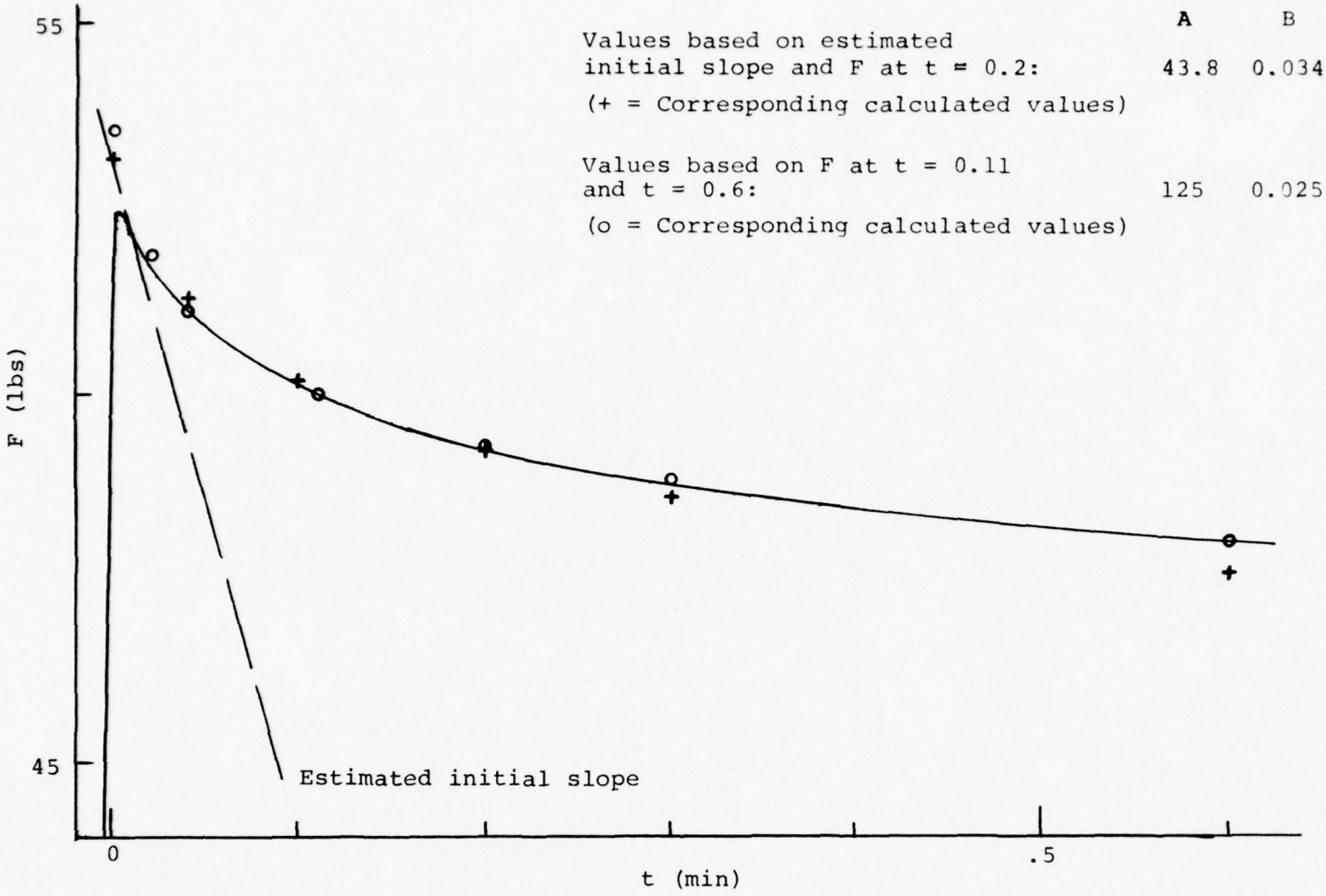

Fig. 3.1.2A Comparison of actual relaxation behavior of PC, indented to a depth of 3.9 mils at 0.02 in/min, compared with results from empirical law using constants determined by two separate procedures.

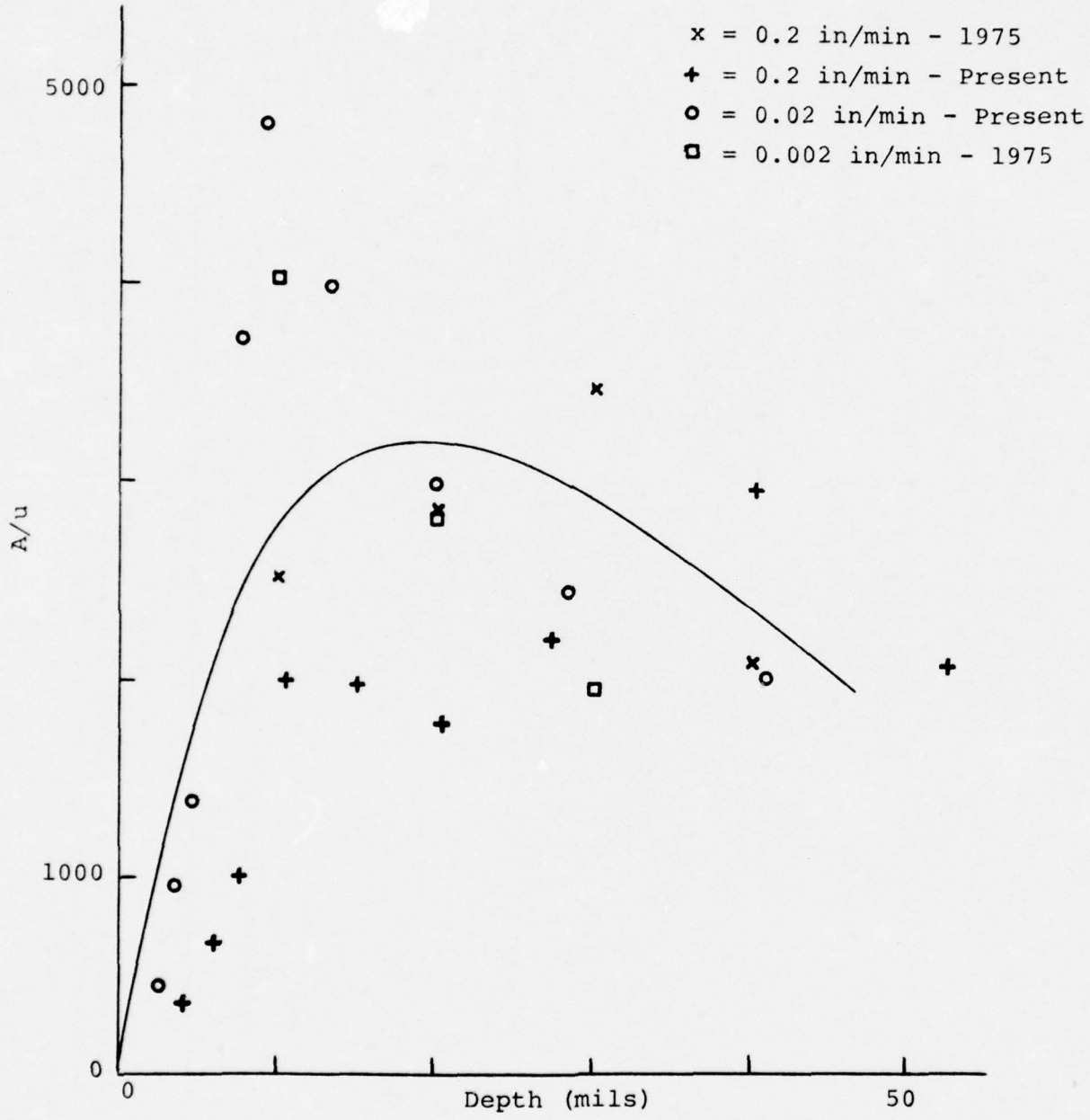

Fig. 3.1.2.1A A/u parameters for PC as a function of indentation depth for various indentation velocities.

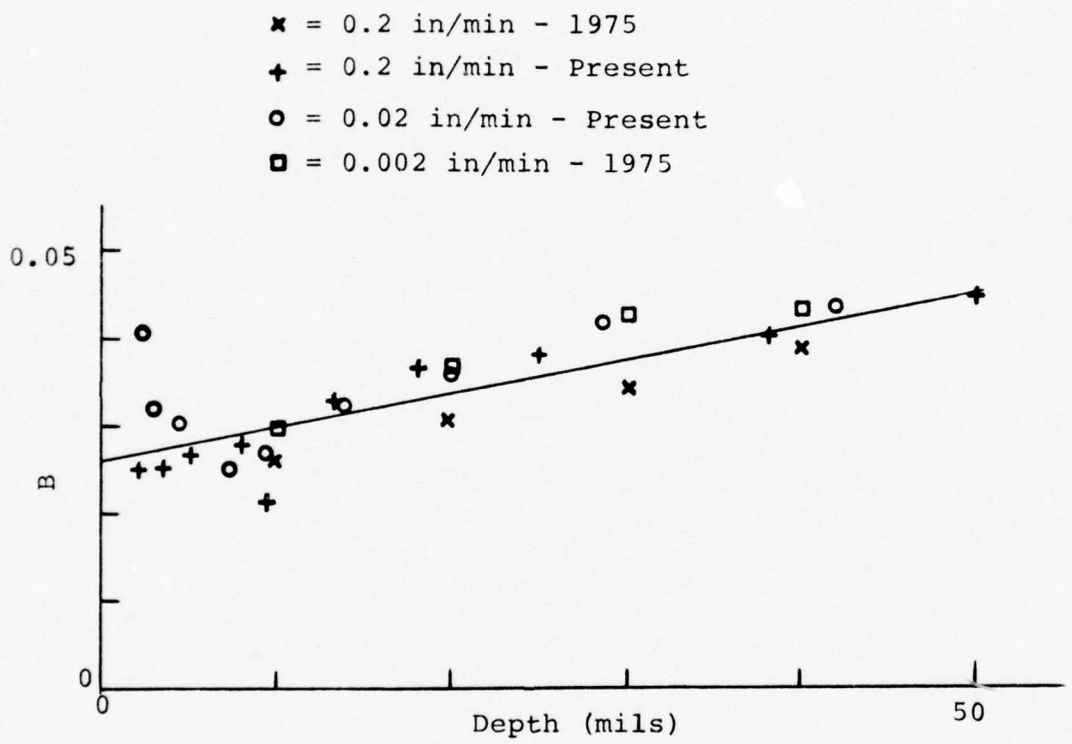

Fig. 3.1.2.1B B parameters for PC as a function of indentation depth for various indentation velocities.

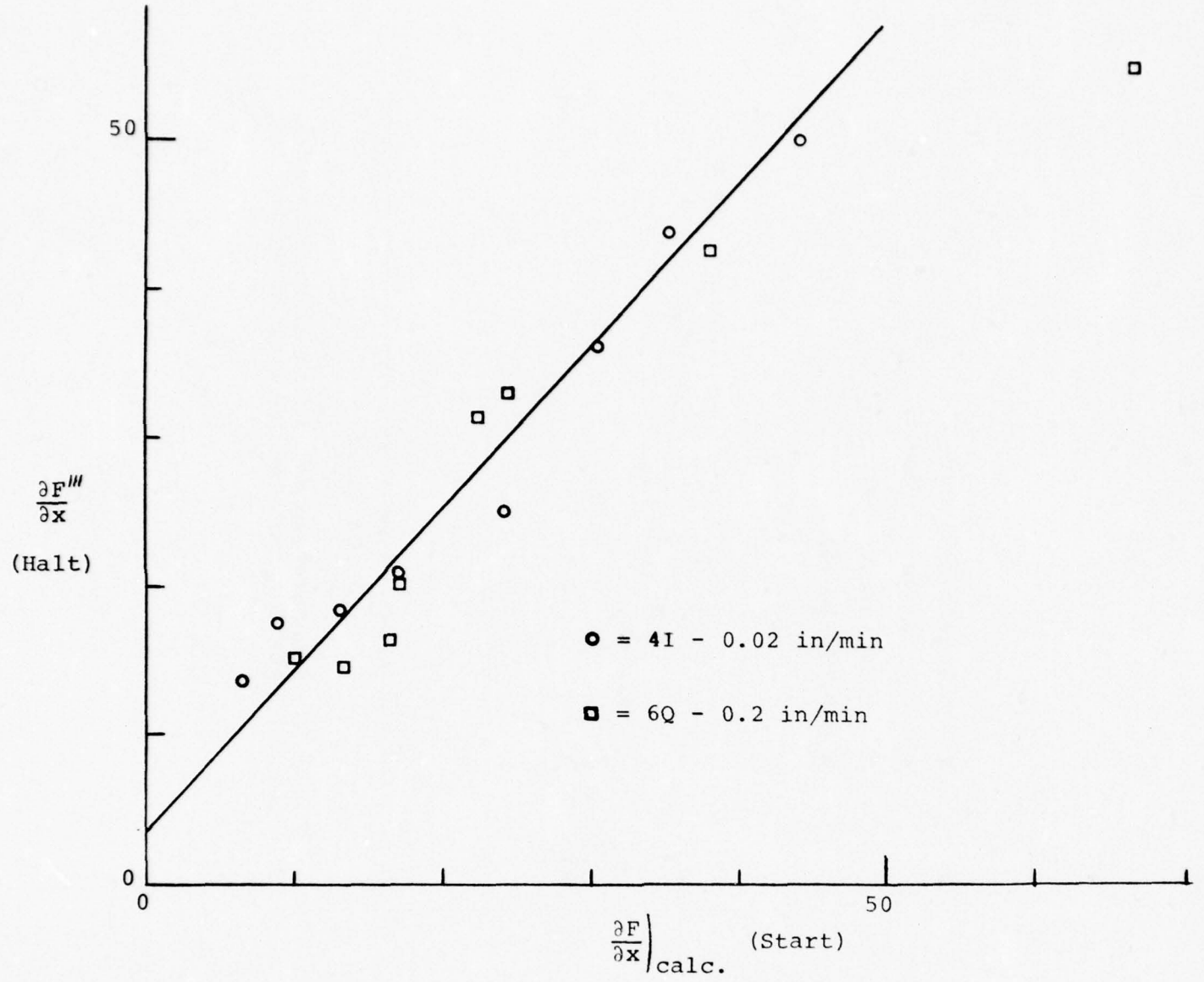

Fig. 3.1.2.1C Comparison of relaxation-corrected $\partial F/\partial x$ for PC at instant of stopping indenter motion versus instant of restarting motion.

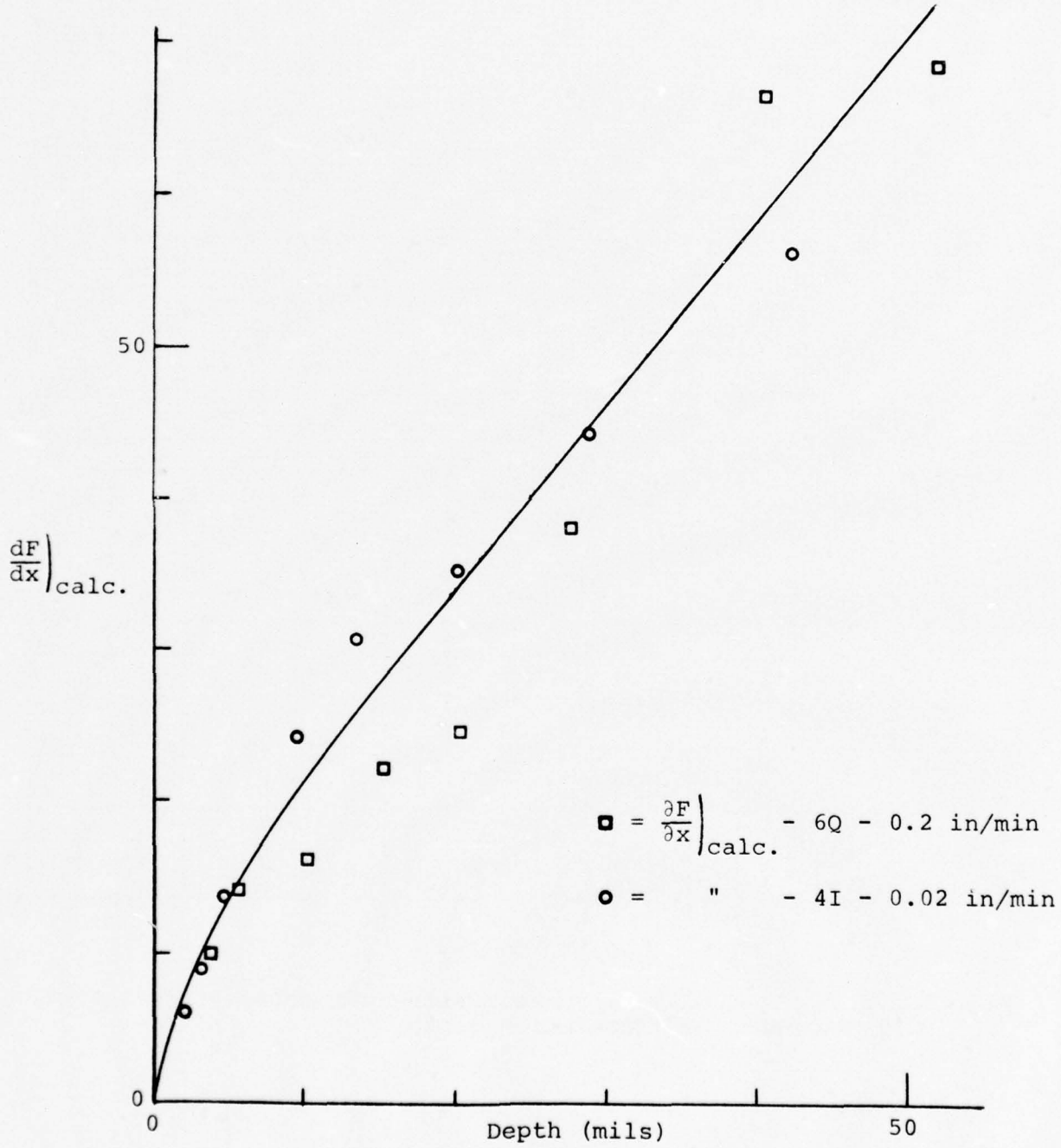

Fig. 3.1.2.1D Relaxation-corrected $\partial F/\partial x$ (start) for PC as function of indentation depth.

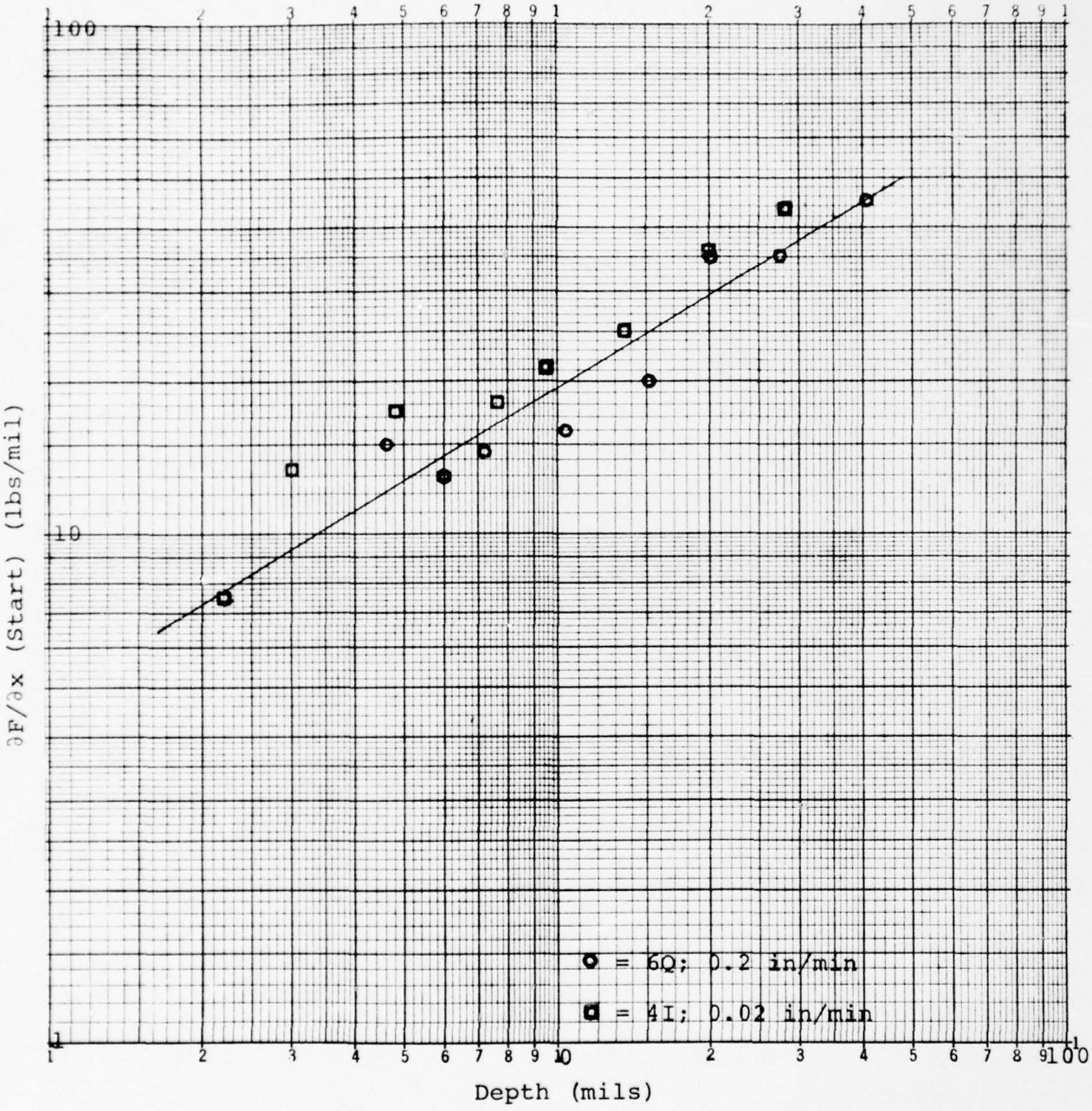

Fig. 3.1.2.1E Log-log plot of relaxation-corrected ∂F/∂x (start) for PC as function of indentation depth.

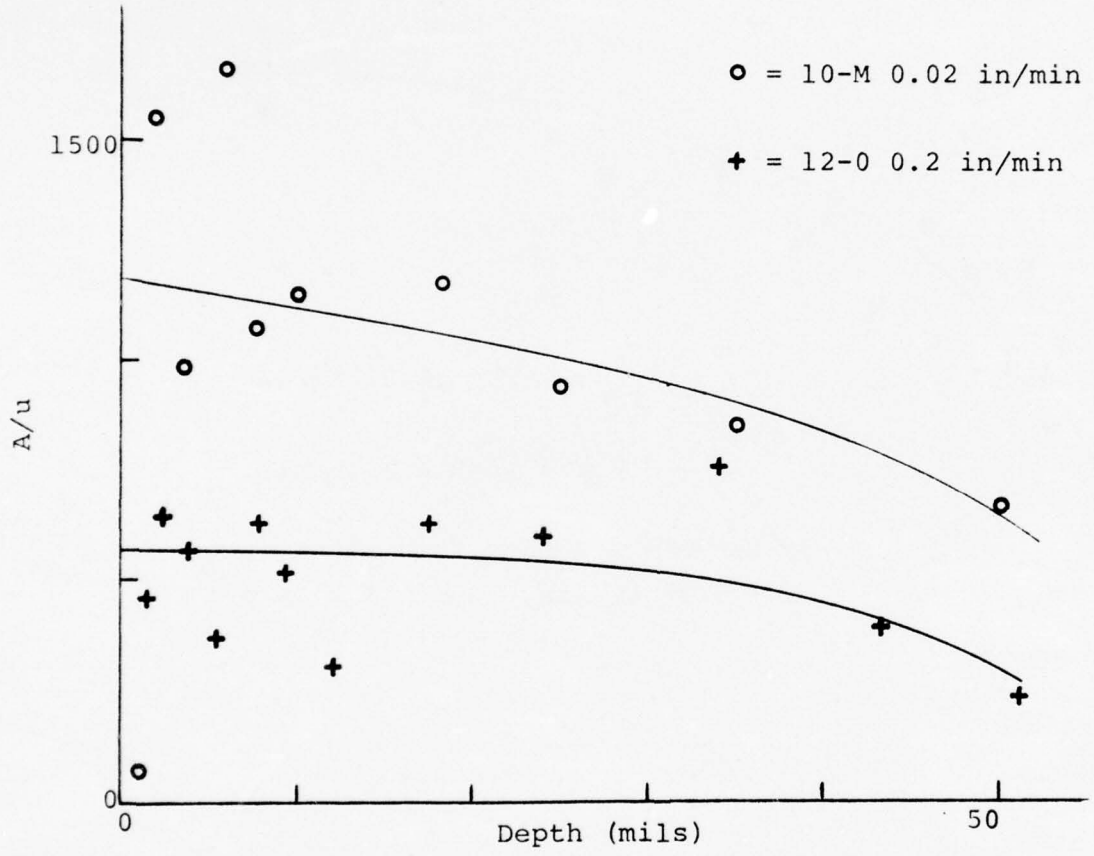

Fig. 3.1.2.2A A/u parameters for PMMA as a function of indentation depth for various indentation velocities.

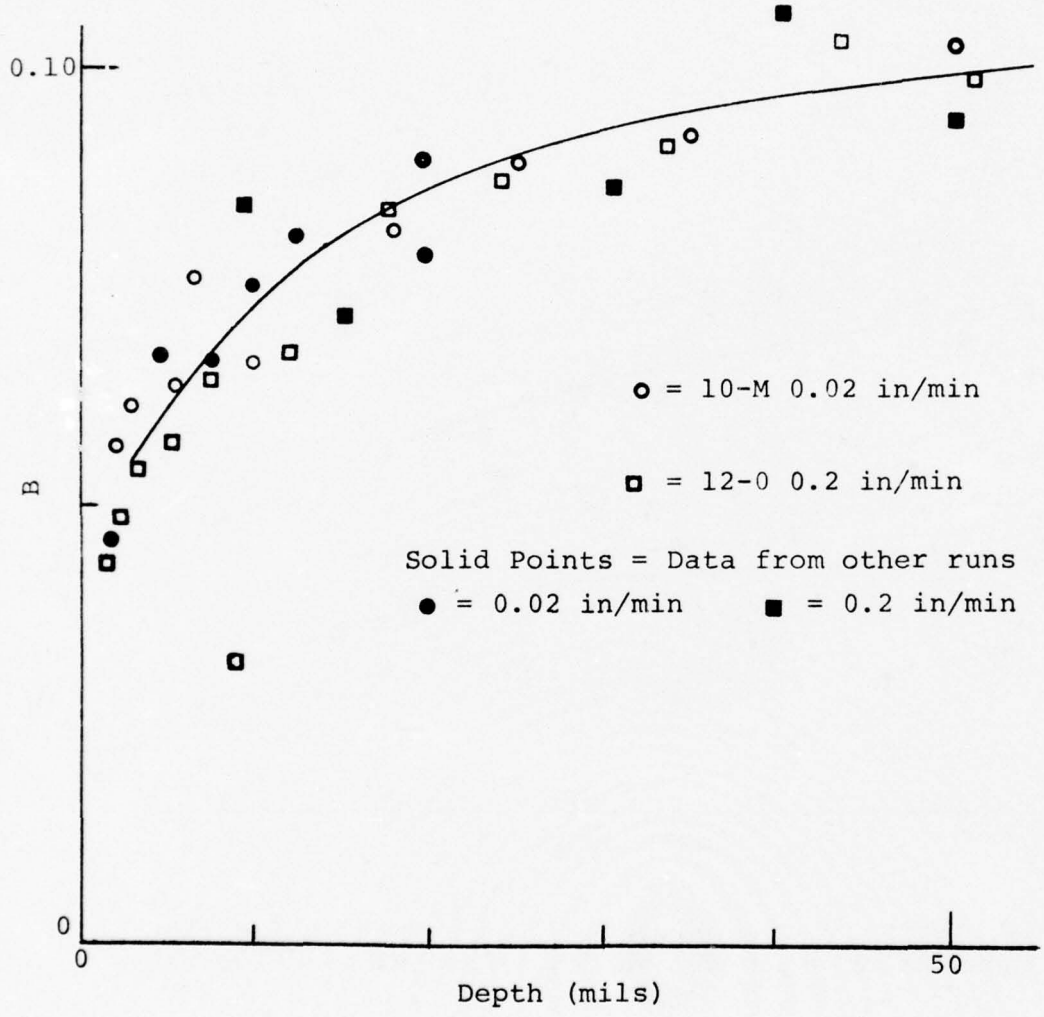

Fig. 3.1.2.2B B parameters for PMMA as a function of indentation depth for various indentatin velocities.

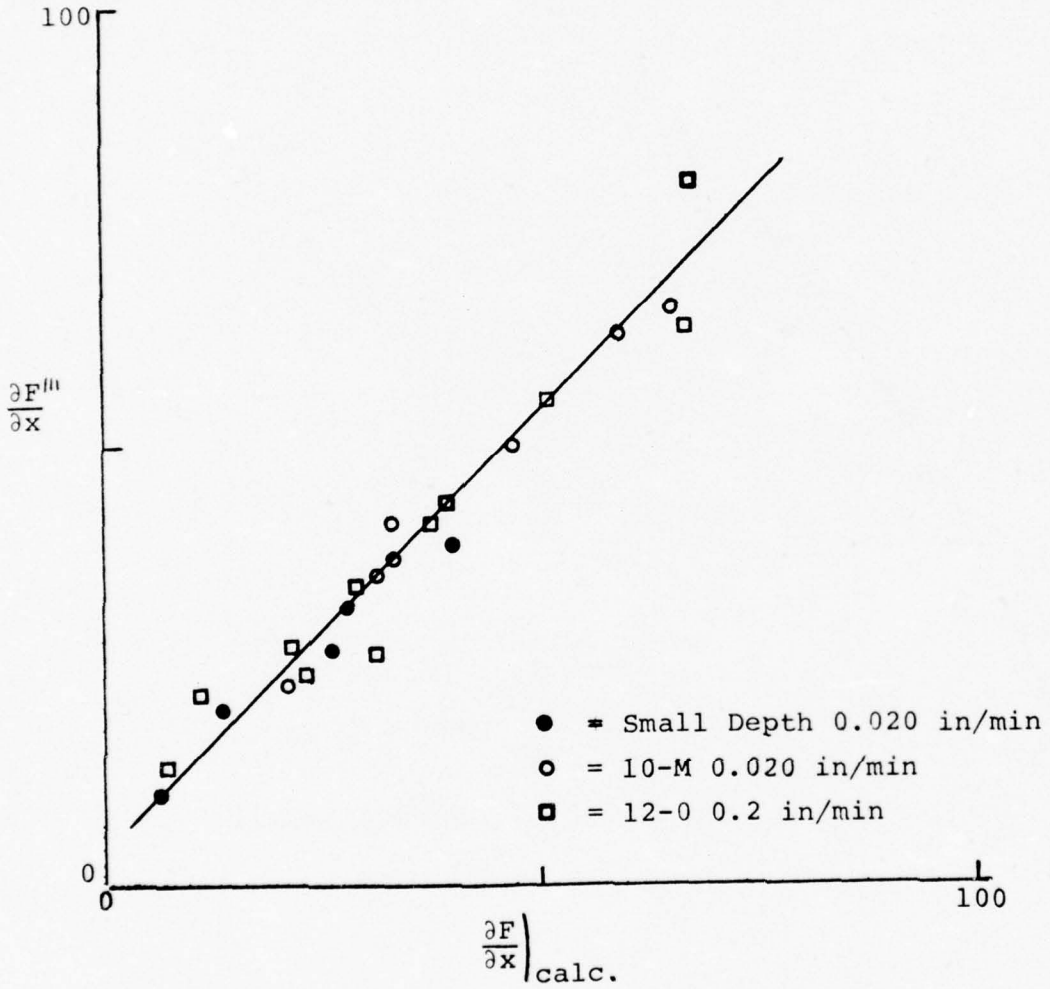

Fig. 3.1.2.2C Comparison of relaxation-corrected $\partial F/\partial x$ for PMMA at instant of stopping. Indenter motion versus instant of restarting motion.

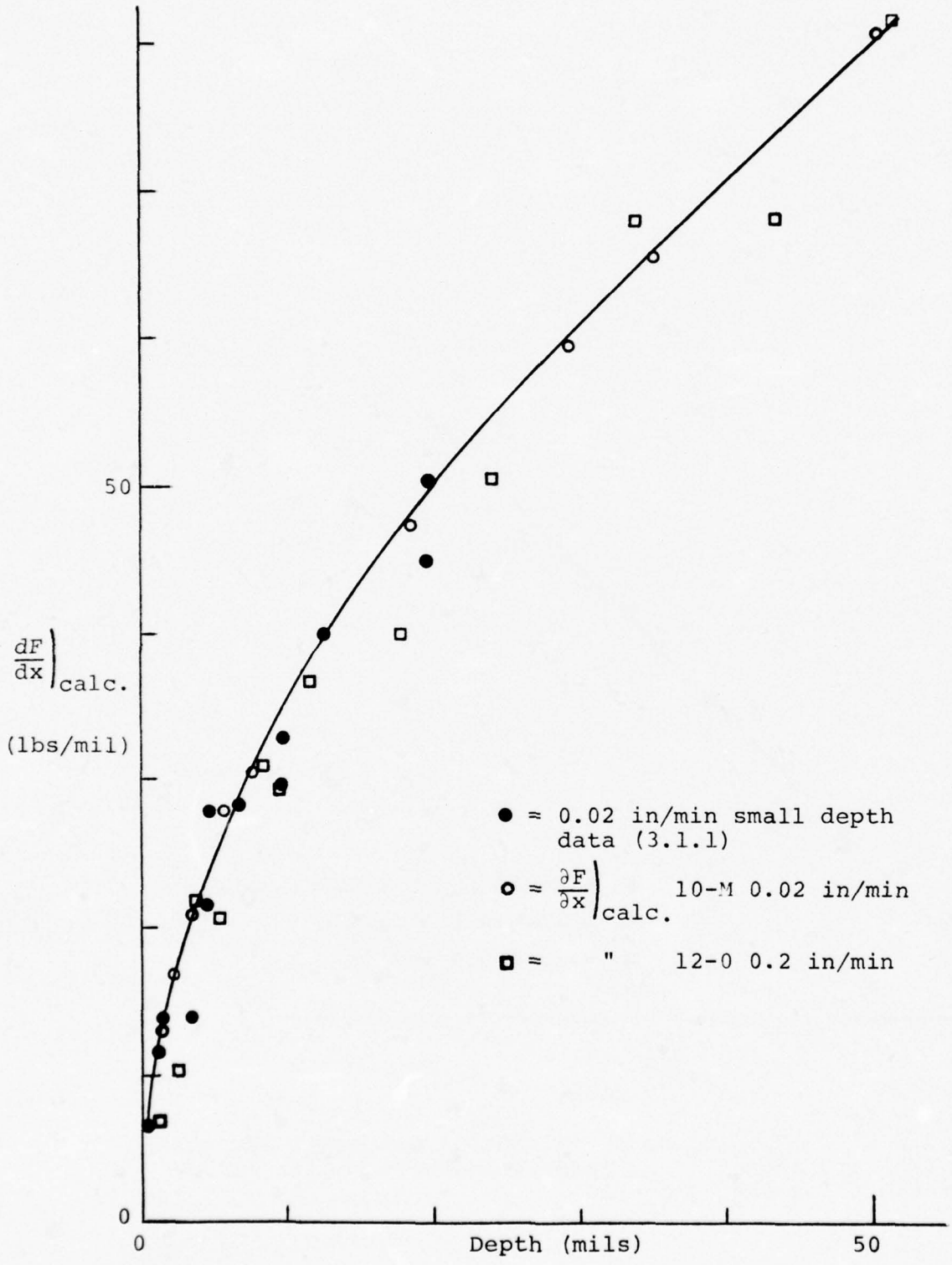

Fig. 3.1.2.2D Relaxation-corrected $\partial F/\partial x$ (start) for PMMA as function of indentation depth.

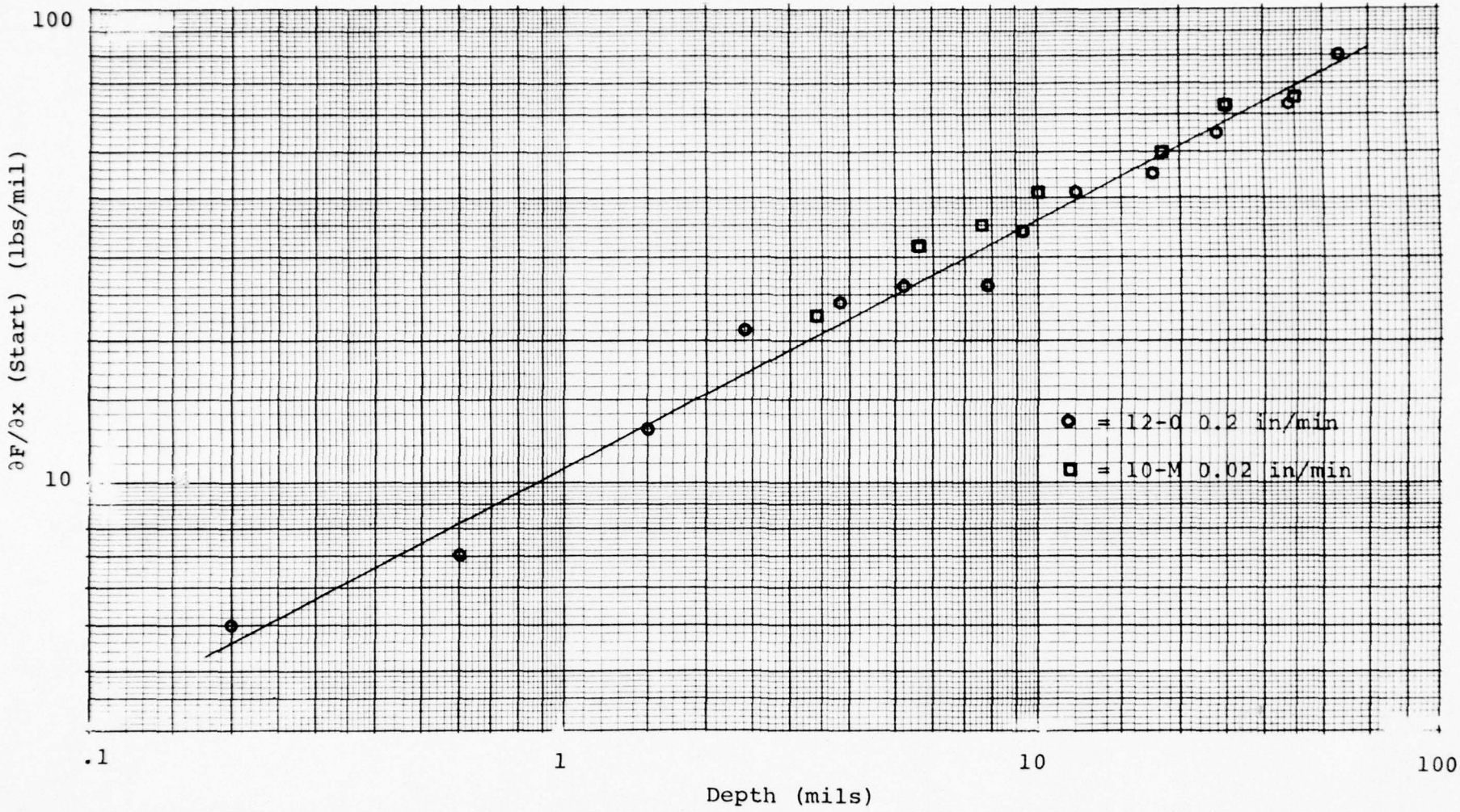

Fig. 3.1.2.2E Log-log plot of relaxation-corrected ∂F/∂x (start) for PMMA as a function of indentation depth.

Fig. 3.1.3A Dependence of relaxation and force parameters on indentation velocity for PC and PMMA.

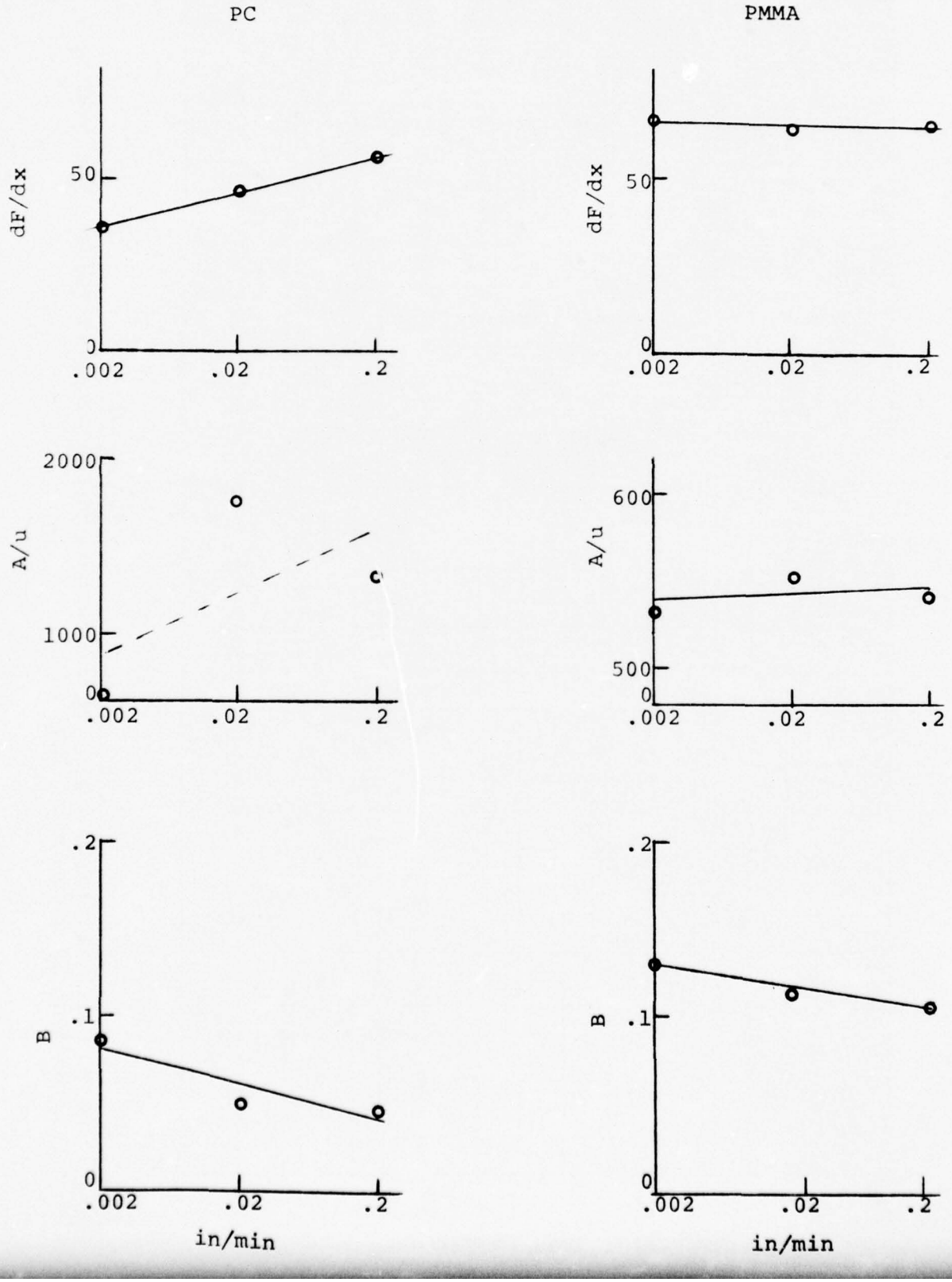

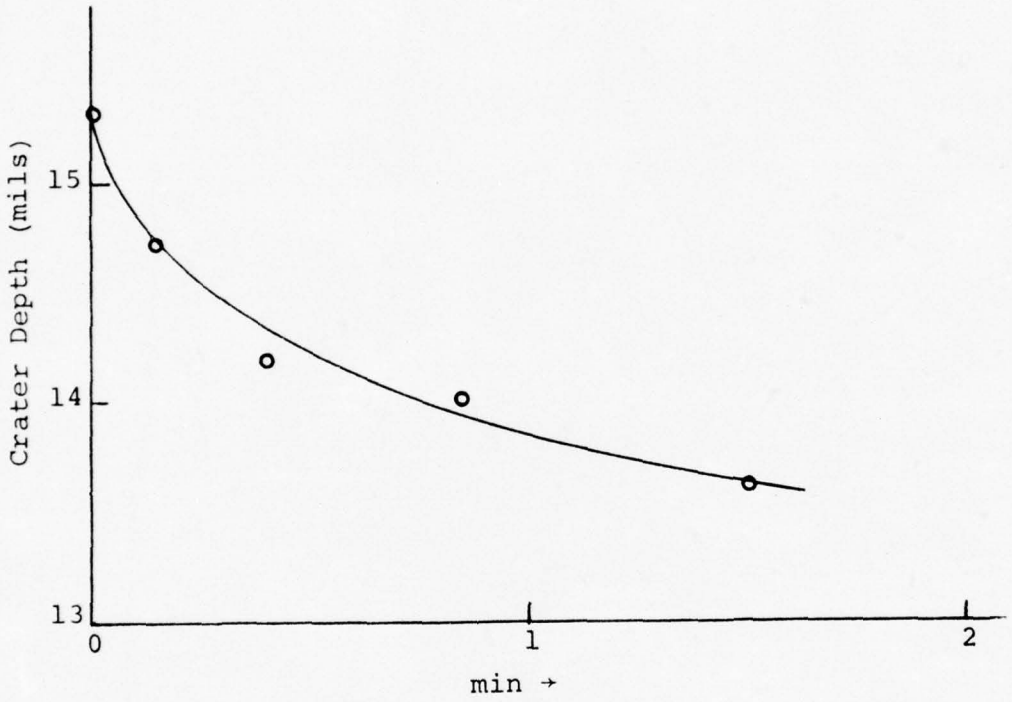

Fig. 3.2A Relaxation of crater depth in PC following the incursion of indenter to 30 mils at 0.02 inches/min

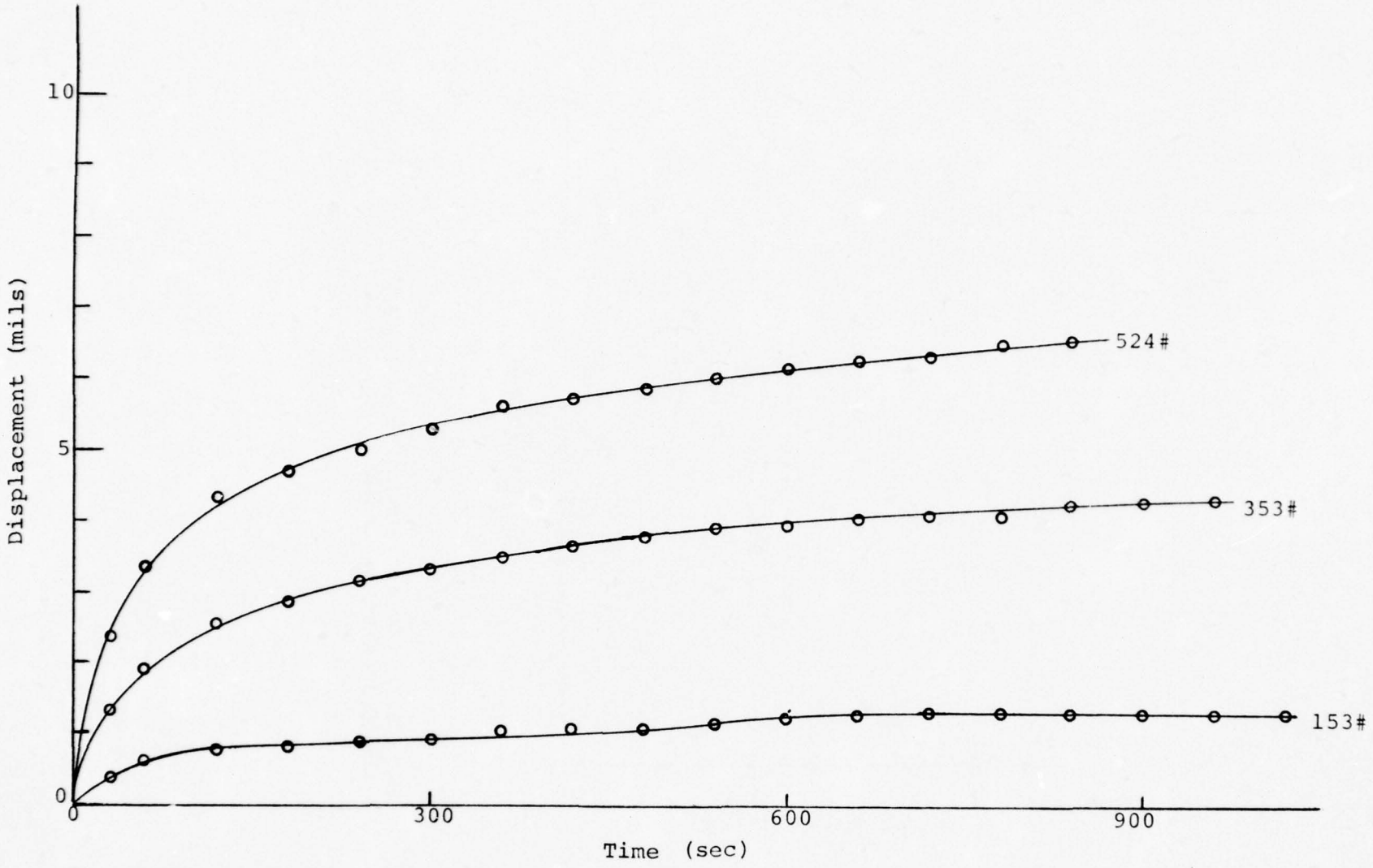

Fig. 3.2B Creep behavior of Lexan being indented with spherical indenter 4.5 mm diameter.

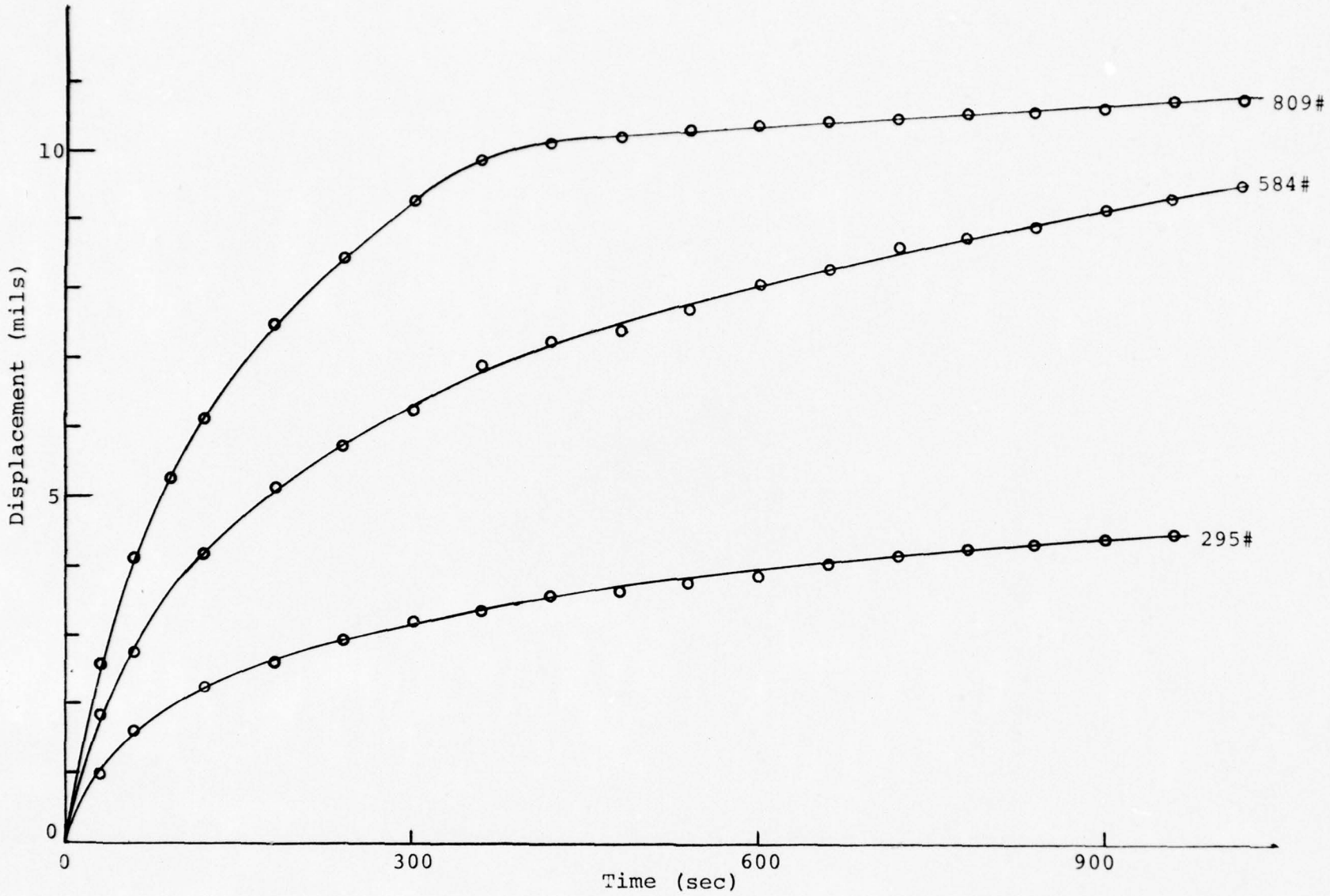

Fig. 3.2C Creep behavior of PMMA being indented with spherical indenter 4.5 mm diameter.

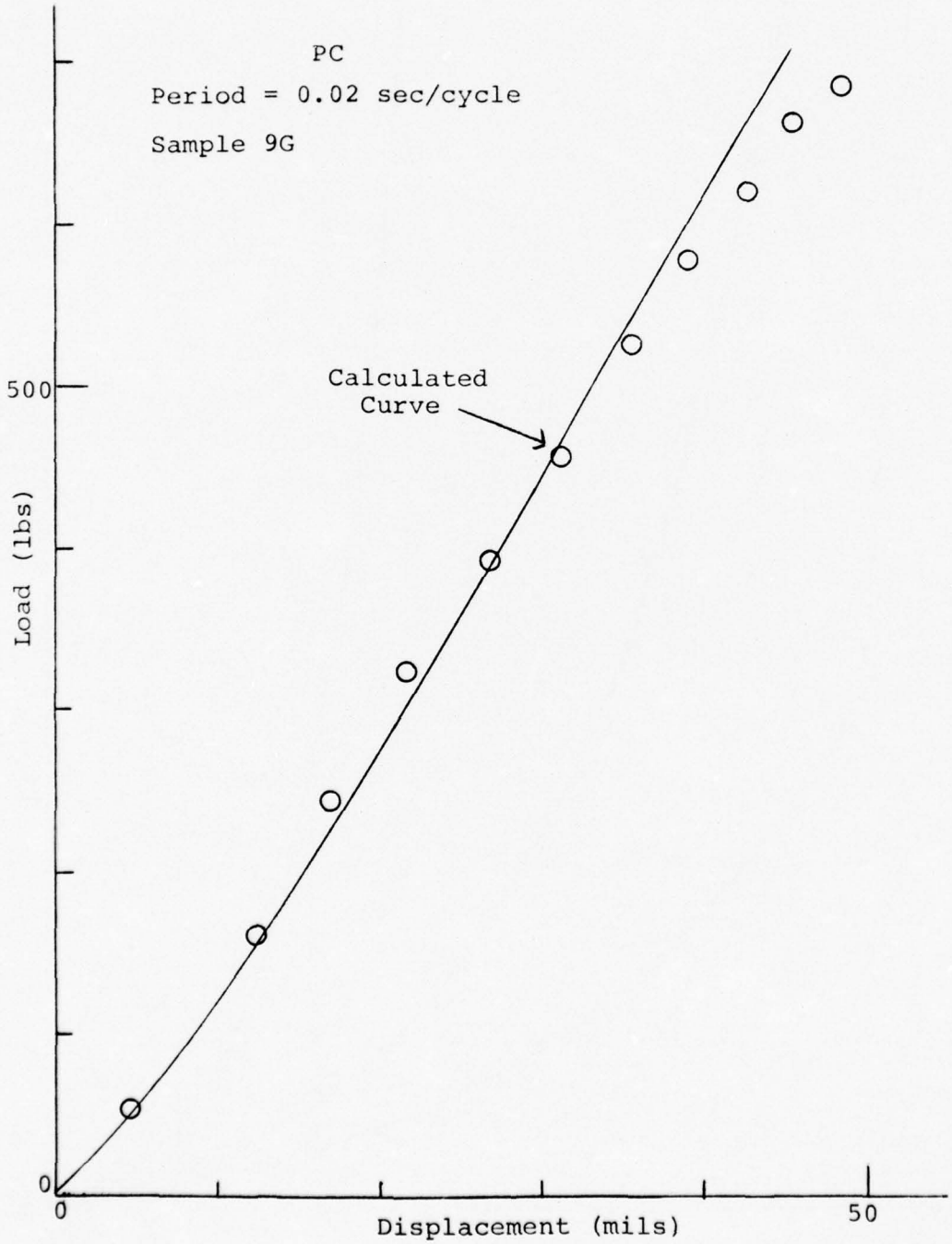

Fig. 3.3A Load versus displacement.

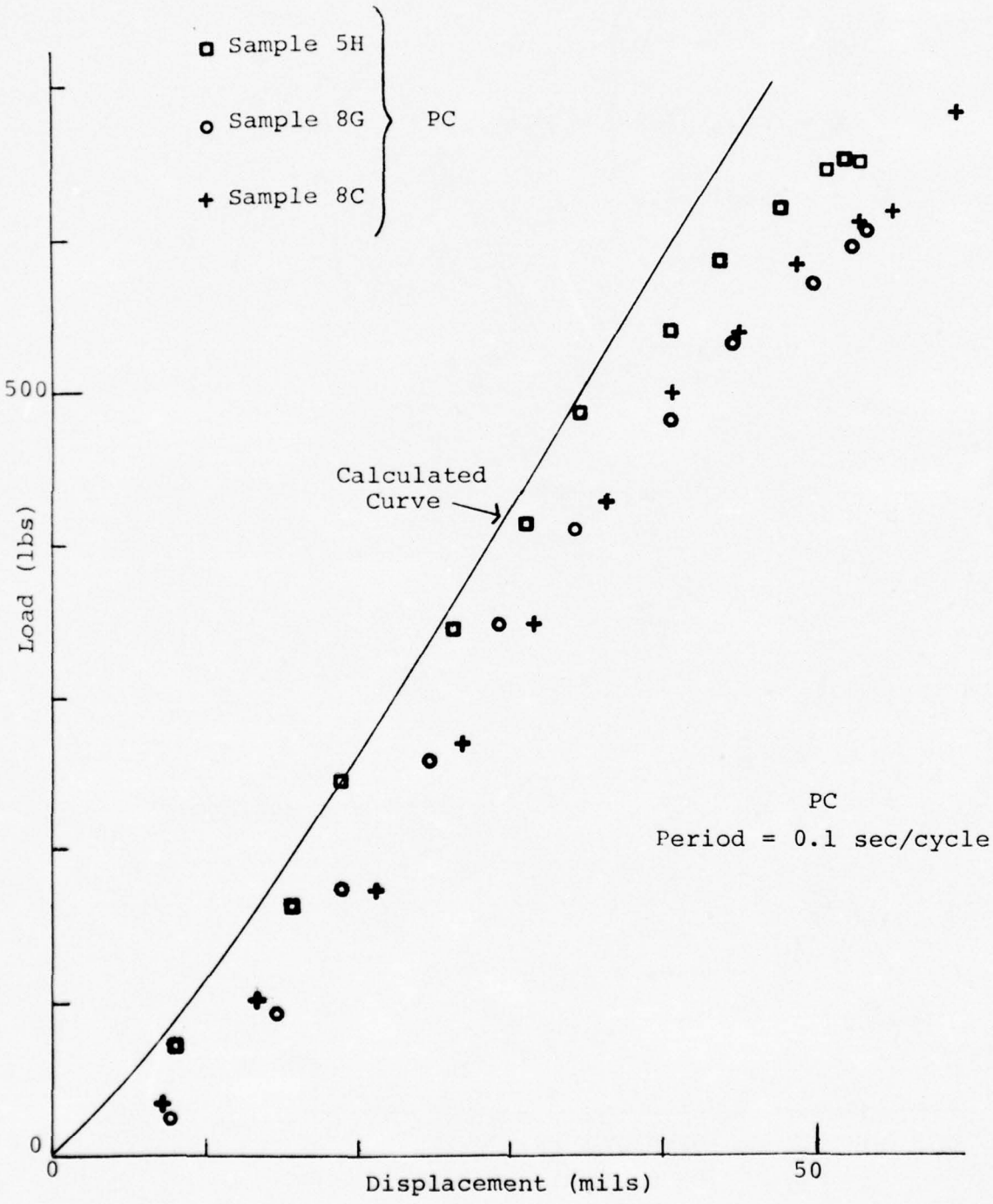

Fig. 3.3B Load versus displacement.

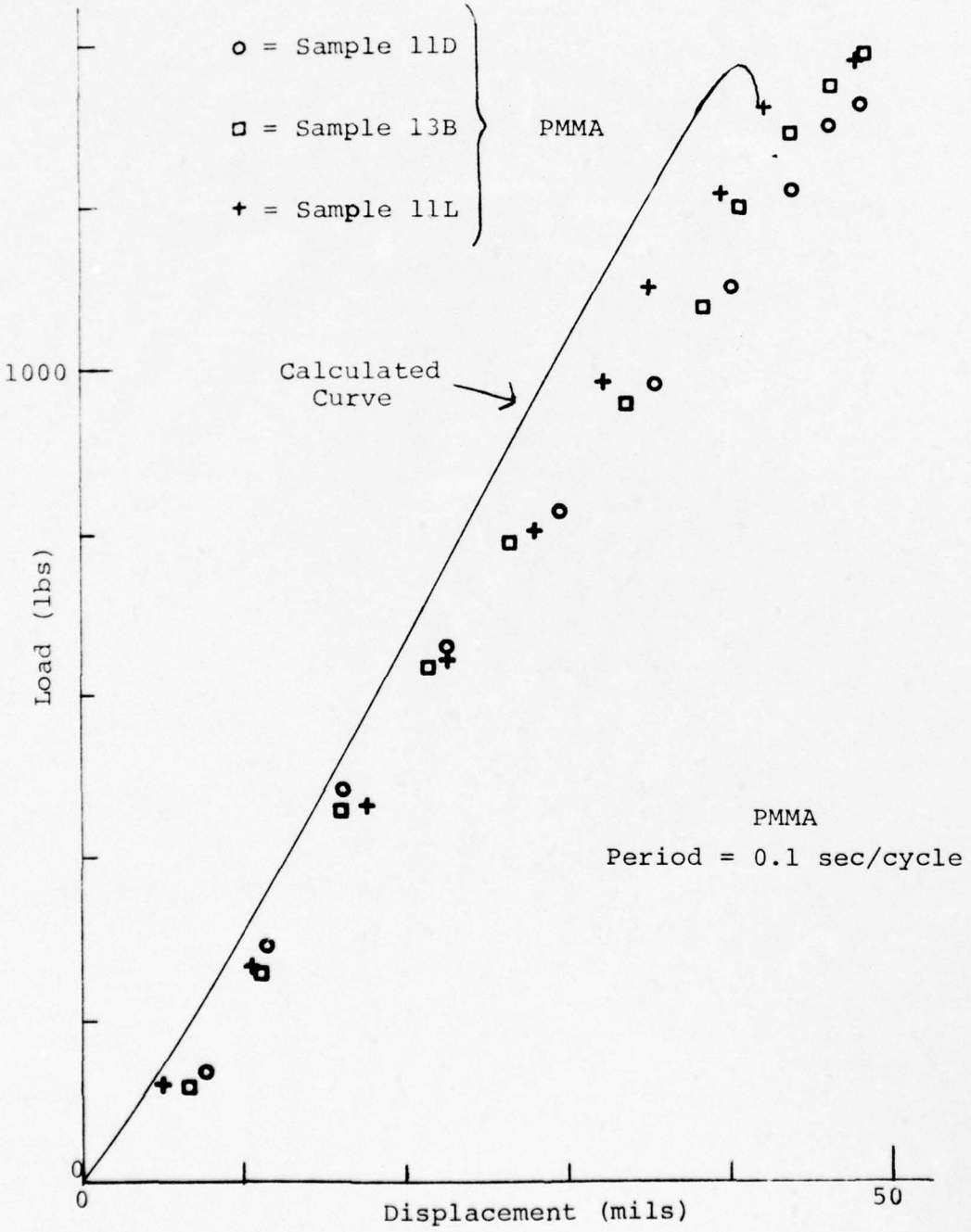

Fig. 3.3C Load versus displacement.

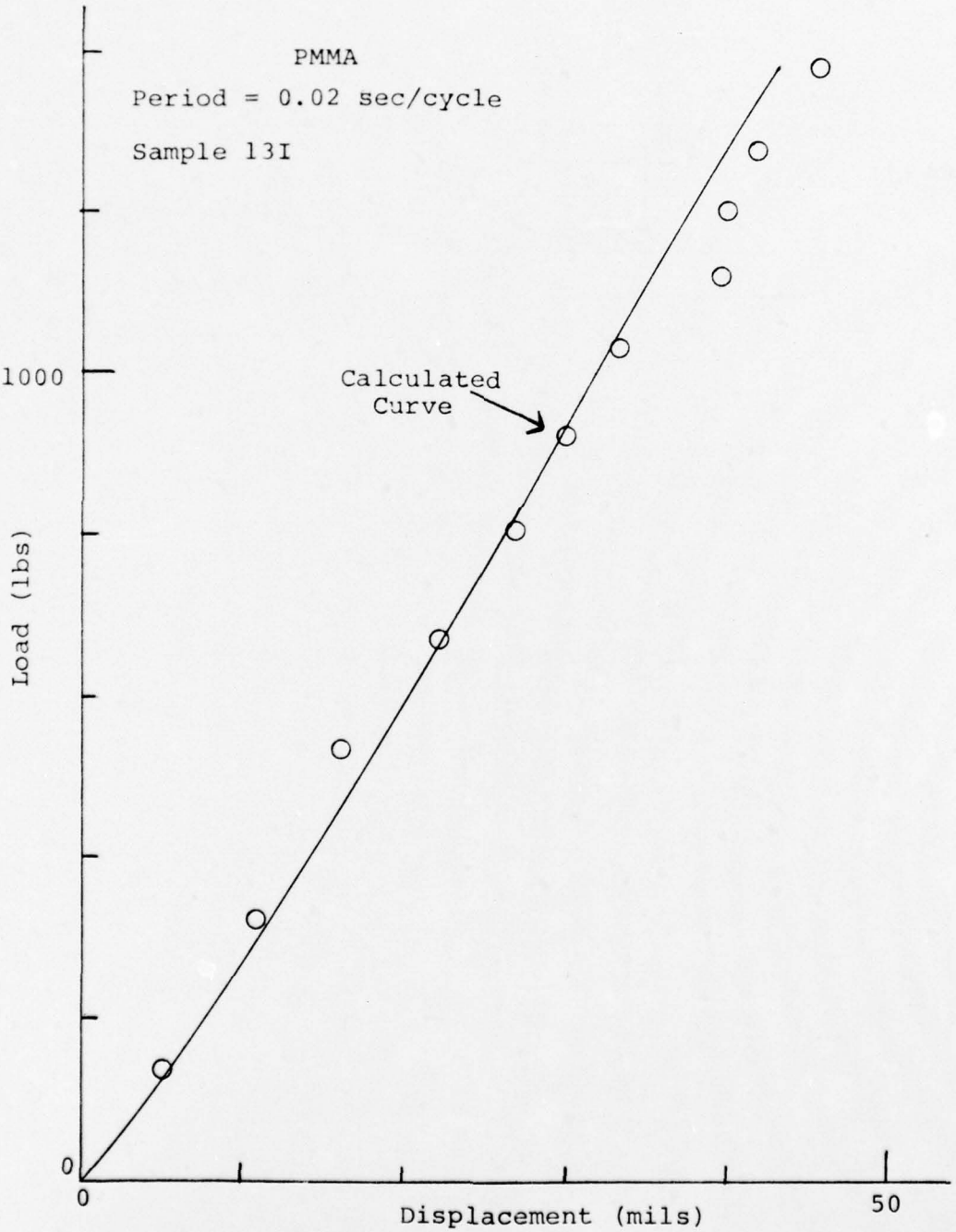

Fig. 3.3D Load versus displacement.

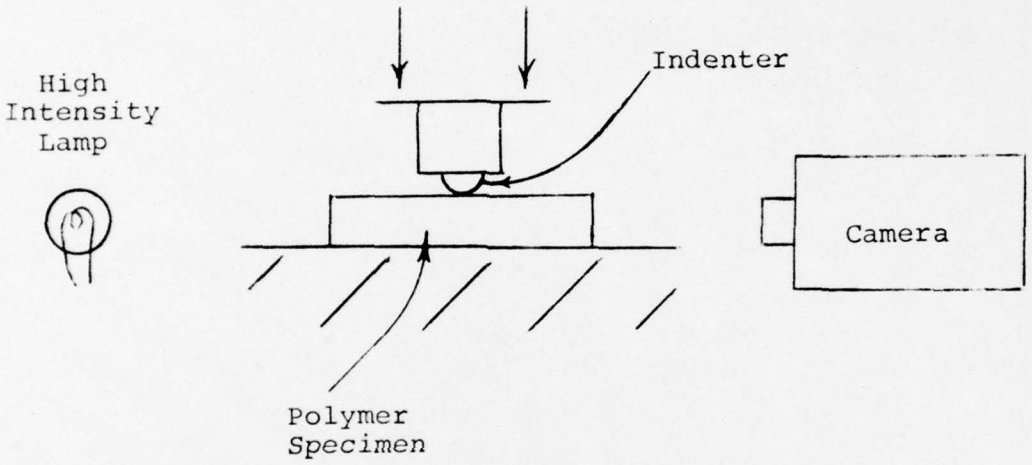

Fig. 4.1A Arrangement for photographing generation of disturbed zone.

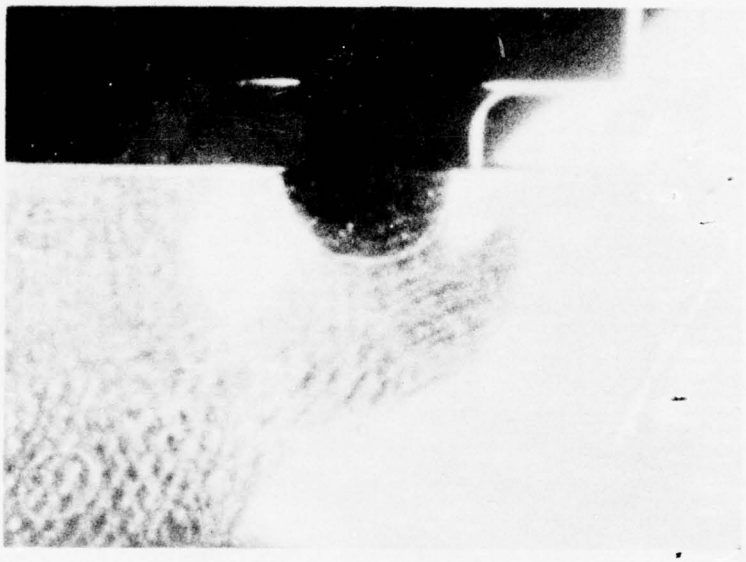

Fig. 4.1B Photograph of the densified zone in PC from motion picture record of the indentation process (∿5.7x).

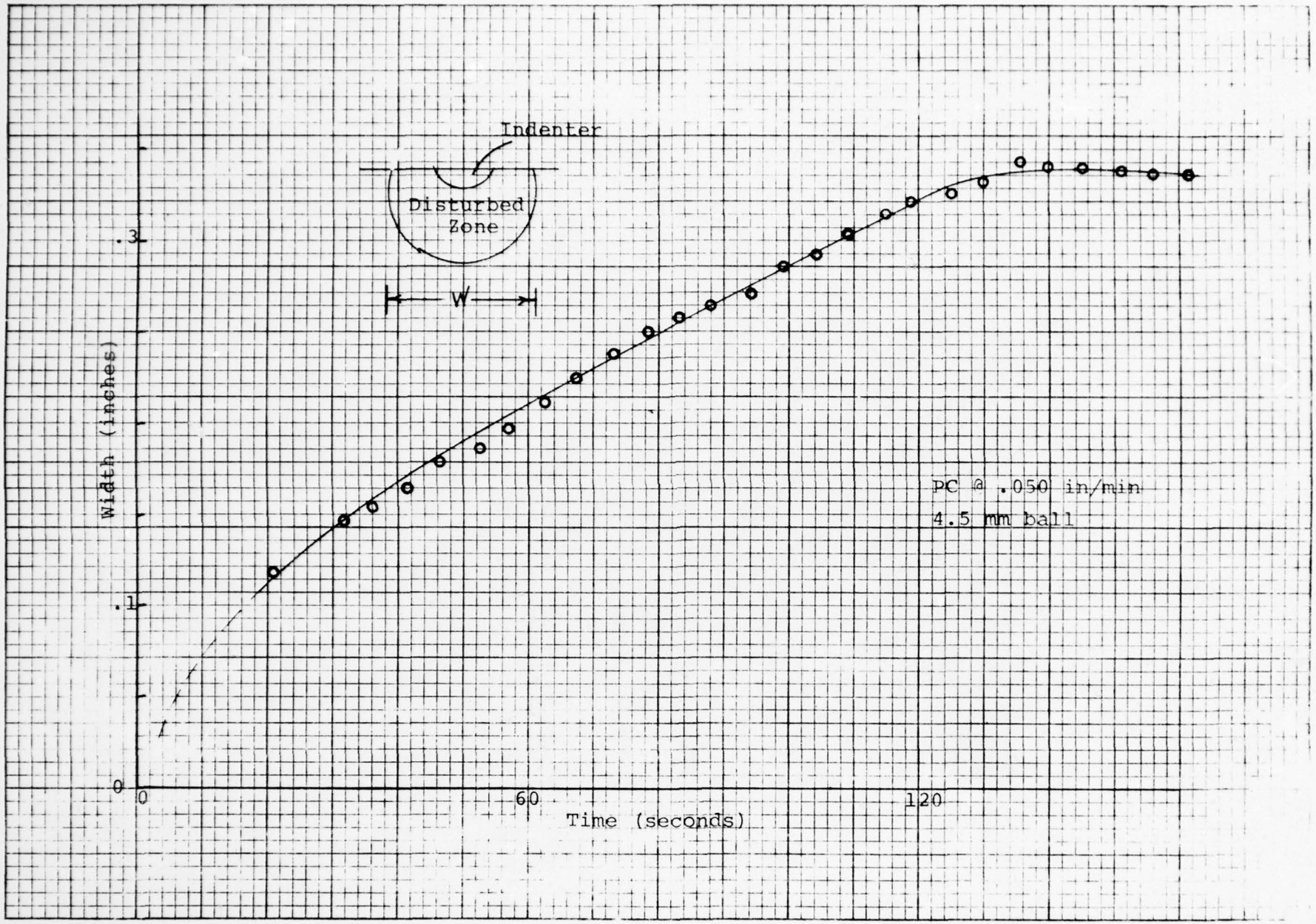

Fig. 4.1C Maximum width of disturbed zone versus time.

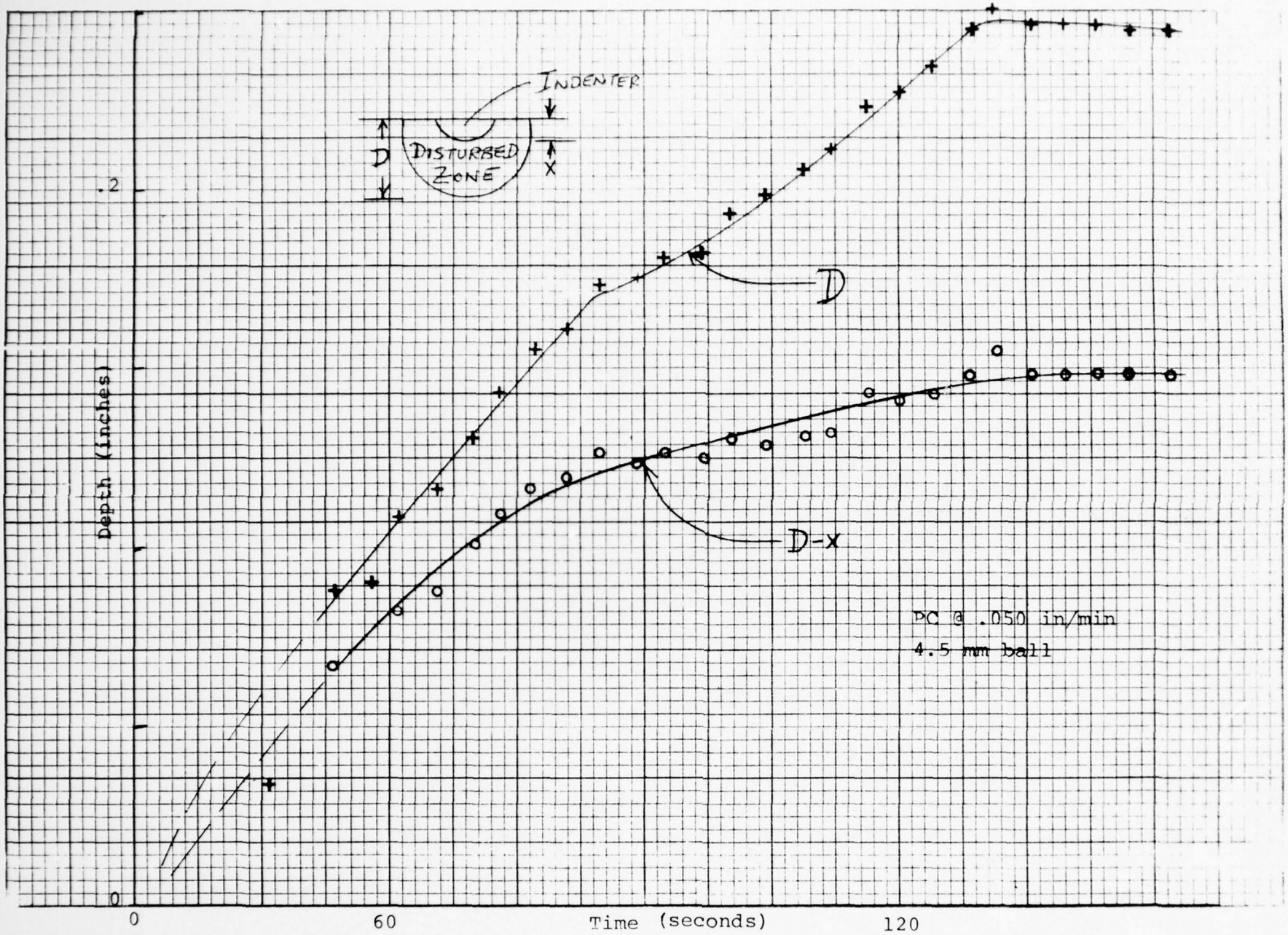

Fig. 4.1D Depth parameter of indentation region versus time.

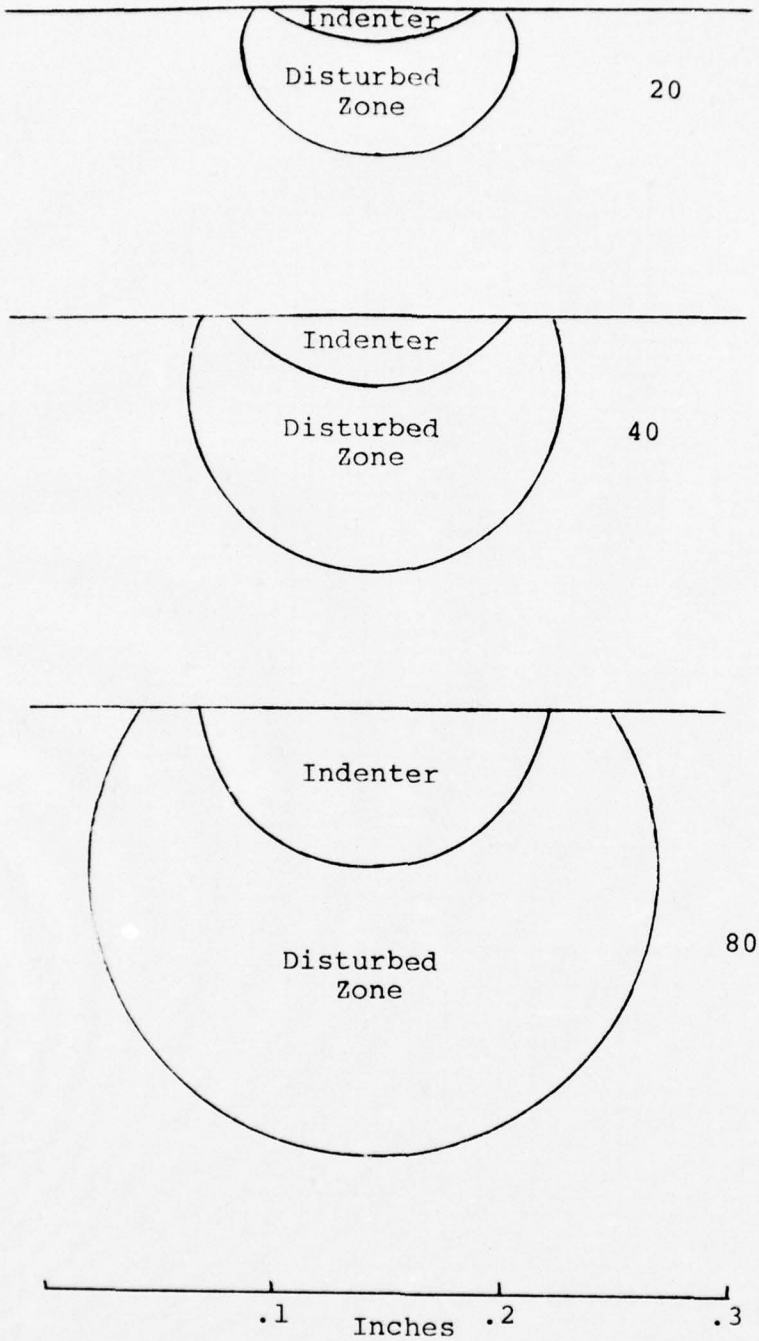

Fig. 4.1E Schematic reconstruction of disturbed region under indenter during indentation of PC at .050 in/min. All drawings to scale indicated.

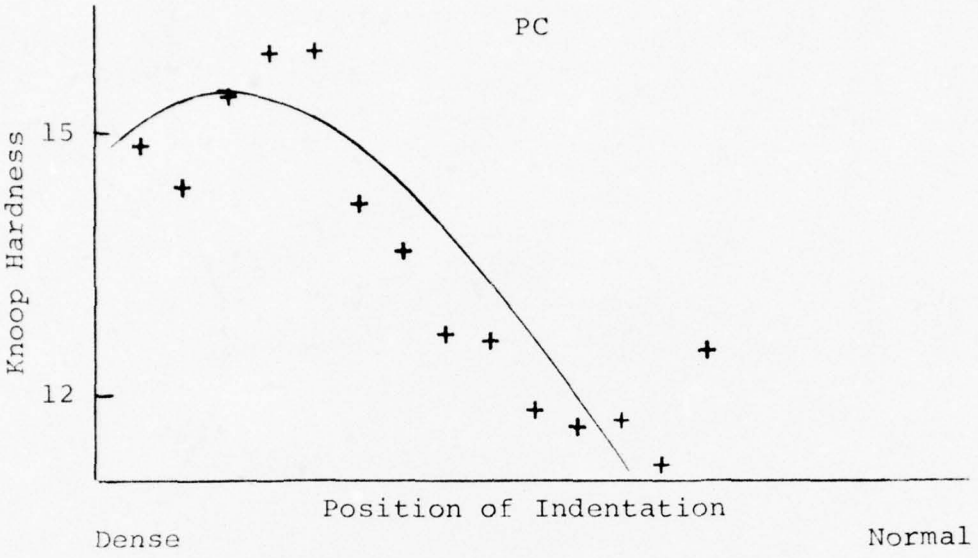

Fig. 4.2A Knoop hardness measurements in PC as function of position moving from disturbed (dense) zone at origin to normal material to right.

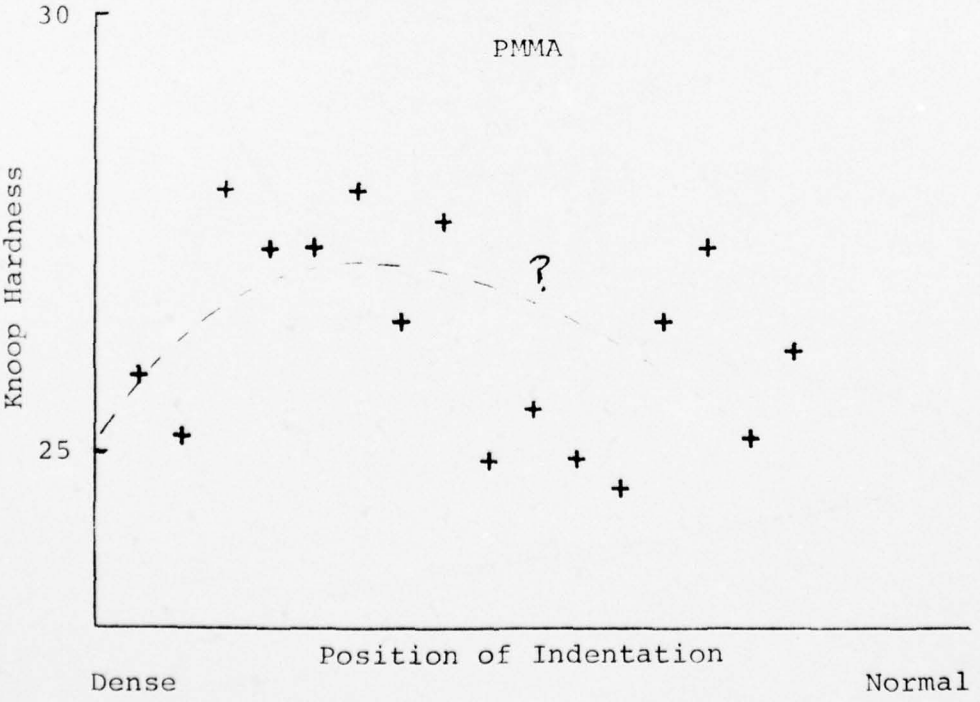

Fig. 4.2B Knoop hardness measurements in PMMA as function of position moving from disturbed (dense) zone at origin to normal material to right.

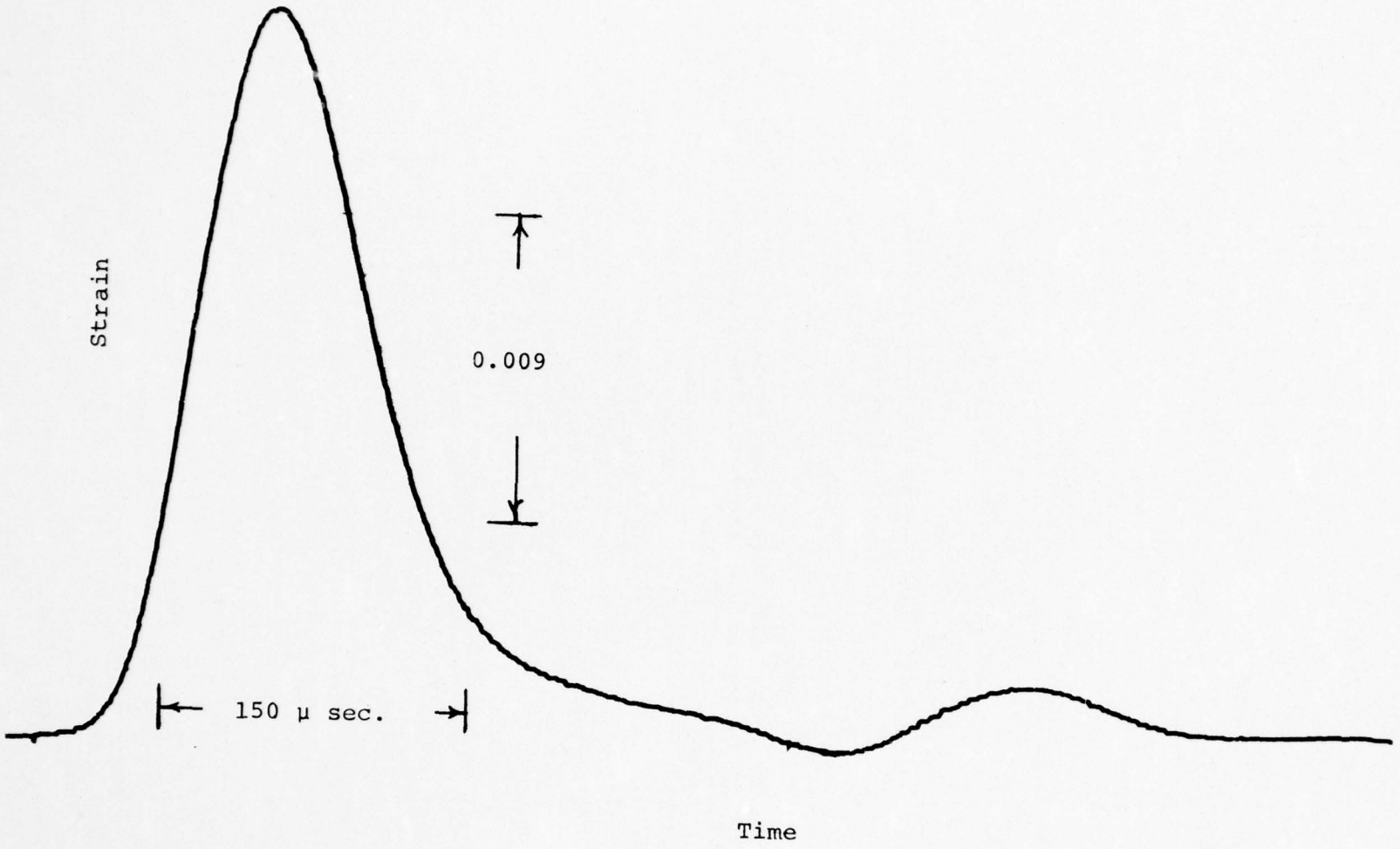

Fig. 5A Strain versus time impact signal produced when 0.75-inch diameter steel projectile strikes end of PMMA bar at 2.8 m/second.

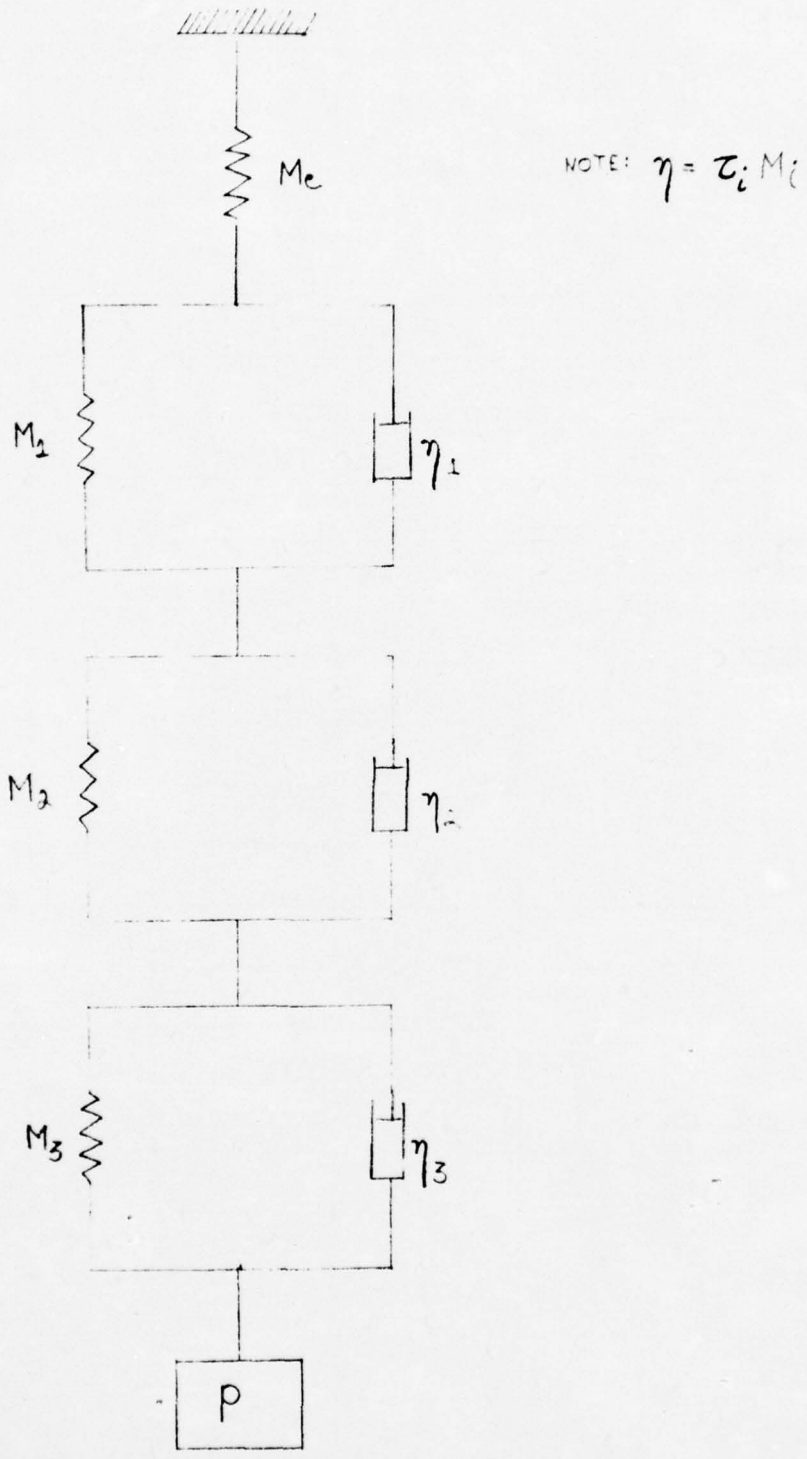

Fig. 6.2A Seven element Kelvin spring-dashpot model.

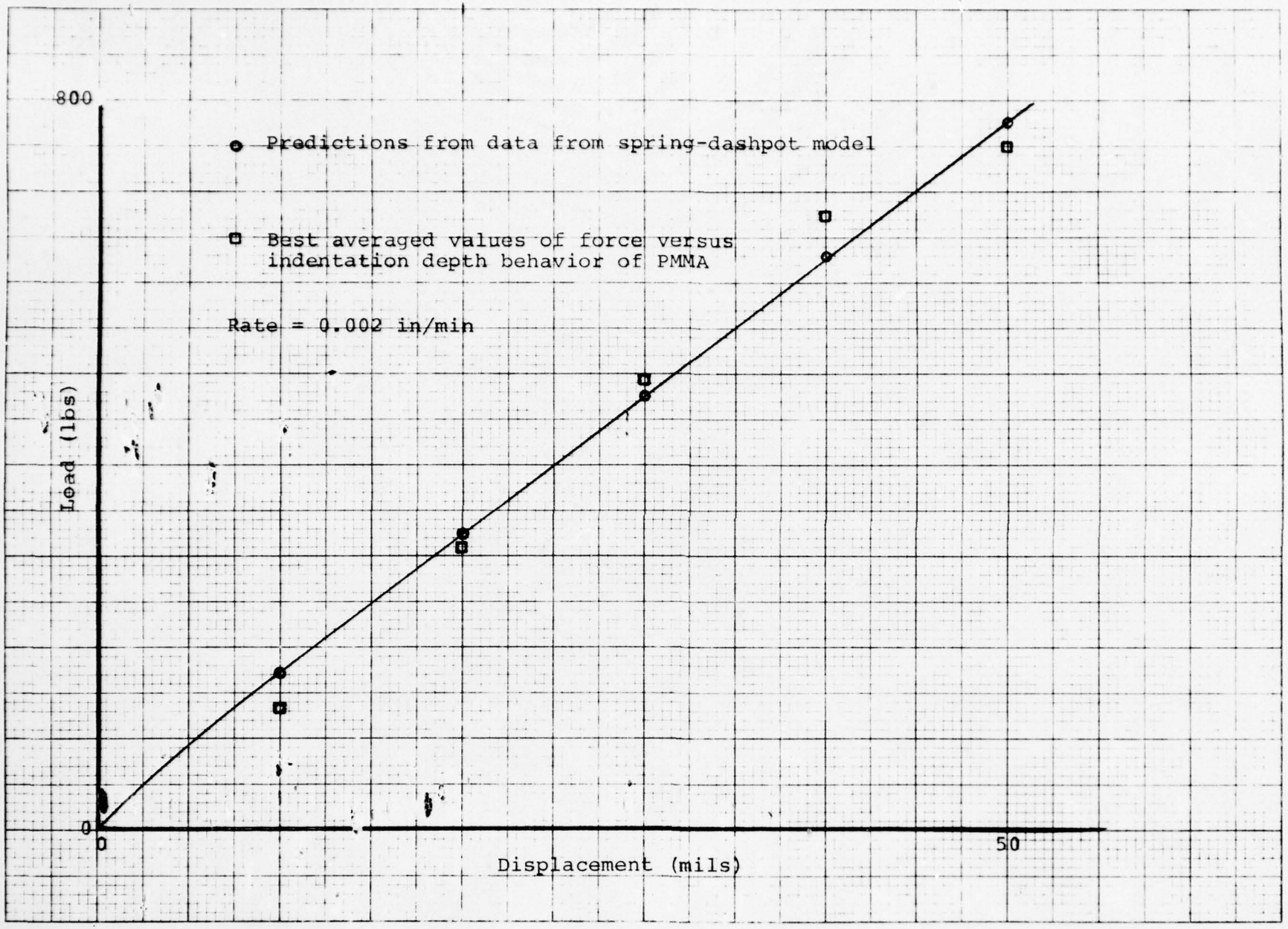

Fig. 6.2B Force versus depth behavior for PMMA at 0.002 in/min indentation rate predicted from creep data using seven element Kelvin model compared with observed behavior.

DISTRIBUTION LIST

Contract No. N00019-75-C-0320

Naval Air Systems Command — 14
Attn: Code AIR-52032
Washington, DC 20361

Naval Air Systems Command — 12
Attn: Code AIR-604
Washington, DC 20361

Office of Naval Research — 3
Washington, DC 20361
Attn: Code 471
Code 472
Code 473

Naval Ordnance Laboratory — 2
White Oak, MD 20910
Attn: Code 2301
Code 234

Materials Sciences & Engineering Laboratory — 1
Stanford Research Institute
Menlo Park, CA 94025

Institute for Materials Research — 3
National Bureau of Standards
Washington, DC 20234

Battelle Memorial Institute — 1
505 King Avenue
Columbus, OH 43201

IIT Research Institute — 1
Attn: Ceramics Division
10 West 35th Street
Chicago, IL 60616

Naval Ship R&D Center — 1
Washington, DC 20007

Naval Ship R&D Center — 1
Annapolis Lab. (Code 287)
Annapolis, MD 21402

Air Force Materials Laboratory — 9
Wright-Patterson Air Force Base
Dayton, OH 45433
Attn: LN 1 LAE 1
LNC 1 LAM 1
LNE 1 LY 1
LNP 1 LT 1
MBC 1 (T.J. Reinhart)

Naval Research Laboratory — 3
Washington, DC 20390
Attn: Code 6000
Code 6100
Code 8433

Atomic Energy Commission — 1
Technical Information Service
P.O. Box 62
Oak Ridge, TN 37830

NASA Headquarters — 1
Attn: B.G. Achhammer
Washington, DC 20546

NASA-Lewis Research Center — 1
Attn: R.F. Lark, Mail Stop 49-1
21000 Brookpark Road
Cleveland, OH 44135

Army Materials & Mechanics Research Center — 3
Watertown, MA 02172
Attn: Dr. R.N. Katz
Dr. G. Thomas
Dr. R. Lewis
Materials Science Lab.

U.S. Army Aviation Material Laboratories — 1
Fort Eustis, VA 23604

Effects Technology, Inc. — 1
Attn: F.R. Tuler
P.O. Box 30400
Santa Barbara, CA 93105

Naval Undersea R&D Center 1
San Diego, CA 92117

Engineering Experiment Station 1
Georgia Institute of Technology
Atlanta, GA 30332

Goodyear Aerospace Corporation 1
Attn: G. Wintermute
Litchfield Park, AZ 85340

Pratt & Whitney Aircraft Div. 1
United Aircraft Corporation
Attn: C. C. Goodrich
East Hartford, CT 06108

TRW Equipment Lab 1
23555 Euclid Avenue
Cleveland, OH 44117

Aero-Electronic Technology Dept. 1
Attn: George Tatnall
Naval Air Development Center
Warminster, PA 18974

Vought Aeronautics Division 1
Attn: A.E. Hohman, Jr.
LTV Aerospace Corporation
P.O. Box 5907
Dallas, TX 75222

Whittaker Corporation 1
Research & Development Division
3540 Aero Court
San Diego, CA 92123

Bell Aerosystems Company 1
Attn: N.E. Wahl
Buffalo, NY 14240

Hydronautics, Incorporated 1
Pindell School Road
Howard County
Laurel, MD 20810

Brunswick Corporation 1
Marion, VA 24354

Plastics Technical Evaluation 1
Center
Picatinny Arsenal
Dover, NJ 07801

Dr. Olive Engel 1
University of Dayton
300 College Park Avenue
Dayton, OH 45409

University of Michigan 1
Attn: F.G. Hammitt
Dept. of Nuclear Engineering
Ann Arbor, MI 48104

Olin Corporation 1
Chemicals Group
New Haven, CT 06540

Aerospace Corporation 1
Materials Laboratory
P.O. Box 95085
Los Angeles, CA 90045

Air Force Avionics Laboratory 1
Wright Patterson AFB
Dayton, OH 45433
Attn: AVTL

U.S. Army Research Office 1
Box CM, Duke Station
Durham, NC 27706

Applied Technology Division 1
Avco Corporation
Lowell Industrial Park
Lowell, MA 01851

Solar Division 1
Attn: Dr. A.G. Metcalfe
International Harvester Company
2200 Pacific Highway
San Diego, CA 92112

Material Sciences Corporation
17777 Walton Road
Blue Bell, PA 19422 — 1

University of Illinois — 1
Attn: Prof. H. T. Corten
Dept. of Theoretical & Applied Mechs.
Urbana, IL 61801

Naval Ship Engineering Center — 1
Attn: Code 6101E
Washington, DC 20361

Westinghouse Research Labs. — 1
Attn: R. Bratton
Beulah Road
Pittsburgh, PA 15235

E. I. duPont deNemours & Company — 1
Attn: C. Zweben, Bldg. 262
Textile Fibers Dept.
Carothers Research Lab
Experimental Station
Wilmington, DE 19898

NTDSC — 1
Southwest Research Institute
P. O. Drawer 28510
San Antonio, TX 78284

Texas A&M University — 1
Attn: Prof. J. L. Rand
Aerospace Engineering Dept.
College Station, TX 77843

Dr. George C. Chang — 1
U. S. Naval Academy
Annapolis, MD 21402

Prof. D. Uhlmann — 1
Massachusetts Institute of Technology
Cambridge, MA 02139

Dr. S. S. Sternstein — 1
Rensselaer Polytechnic Institute
110 8th Street
Troy, NY 12181

Prof. R. Doremus — 1
Rensselaer Polytechnic Institute
110 8th Street
Troy, NY 12181

Prof. M. Goldstein — 1
Belfer Graduate School
Yeshiva University
500 W. 185 Street
New York, NY 10033 — 1

John D. Ferry — 1
Department of Chemistry
University of Wisconsin
Madison, WI 53706 — 1

Dr. A. B. Bestul — 1
National Bureau of Standards
Washington, DC 20234

Prof. J. H. Gibbs — 1
Metcalf Chem. Lab. — 1
Brown University
Providence, RI 02912

Polymer Research Institute — 1
Univ. of Massachusetts
Amherst, MA 01002

Dr. T. Alfrey, Jr. — 1
Polymer Research Lab. — 1
Dow Chemical Company
Midland, MI 48640

Prof. N. Brown — 1
Metallurgy Dept.
Univ. of Pennsylvania
Philadelphia, PA 19104

Dr. S. Krimm 1
Univ. of Michigan
Ann Arbor, MI 48104

R.S. Marvin 1
National Bureau of Standards
Washington, DC 20234

Prof. John F. Fellers 1
Polymer Science & Engineering Program
419 Dougherty Engineering Building
University of Tennessee
Knoxville, TN 37916